NASA TECHNICAL NOTE

NASA TN D-6799

HYPERSONIC AND TRANSONIC BUZZ MEASUREMENTS ON THE LOWER PITCH FLAP OF THE M2-F2 LIFTING ENTRY CONFIGURATION

by Robert W. Warner and Phillip R. Wilcox

Ames Research Center
Moffett Field, Calif. 94035

1. Report No. NASA TN D-6799	2. Government Accession No.	3. Recipient's Catalog No.
4. Title and Subtitle HYPERSONIC AND TRANSONIC BUZZ MEASUREMENTS ON THE LOWER PITCH FLAP OF THE M2–F2 LIFTING ENTRY CONFIGURATION		5. Report Date May 1972
		6. Performing Organization Code
7. Author(s) Robert W. Warner and Phillip R. Wilcox		8. Performing Organization Report No. A–3790
9. Performing Organization Name and Address Ames Research Center Moffett Field, Calif. 94035		10. Work Unit No. 134–14–07–07
		11. Contract or Grant No.
12. Sponsoring Agency Name and Address National Aeronautics and Space Administration Washington, D. C. 20546		13. Type of Report and Period Covered Technical Note
		14. Sponsoring Agency Code

15. Supplementary Notes

16. Abstract

Free-oscillation damping measurements at hypersonic and transonic Mach numbers are presented for the lower pitch flap of a wind-tunnel model of the M2–F2 reentry vehicle. For the hypersonic test, the nominal Mach number is 7.3 the Reynolds number (based on 30.5 cm (1 ft)) ranges from 0.257×10^6 to 4.66×10^6, the angle of attack ranges from -0.105 rad (-6°) to +0.349 rad (+20°), and the mean flap deflections are 0.611 rad (35°) and 1.047 rad (60°) down from the local body contour. For the transonic test, the mean flap deflection is 0.611 rad (35°), the Mach number ranges from 0.85 to 0.99, the Reynolds number (with length as above) from 4.35×10^6 to 4.97×10^6, and the angle of attack from -0.068 rad (-4°) to +0.244 rad (+14°). For the flow and model conditions tested, the damping measurements (together with flow pictures and pressure information) indicate the absence of hypersonic buzz instability for flap rotation frequencies of 47.3 Hz, 153 Hz, and 360 Hz, the presence of transonic buzz for the 47.3 Hz flap, and the absence of transonic buzz for a 115 Hz flap (all with a flap chord length of 4.384 cm (1.726 in.)). There is not enough flap damping data for an error estimate based on repeatability, but a partial damping calibration is presented in which an analog computer simulation of the random flap response for a known flap damping is fed into the autocorrelation computer and filter combination used for most of the damping measurements.

17. Key Words (Suggested by Author(s)) Flutter Buzz Control surface derivatives Unsteady aerodynamics Hypersonic flow Transonic flow Lifting body Reentry vehicles	18. Distribution Statement Unclassified — Unlimited		
19. Security Classif. (of this report) Unclassified	20. Security Classif. (of this page) Unclassified	21. No. of Pages 48	22. Price* $3.00

NOTATION

c	flap chord (4.384 cm (1.726 in.))
f_n	flap natural frequency (under flow conditions), Hz
f_{no}	flap natural frequency (still air), Hz
$\left.\begin{array}{l} f_{n1}, f_{n2}, \\ f_{n3} \end{array}\right\}$	natural frequencies in analog simulation, Hz
h	vertical distance between spring and hinge flexures (3.607 cm or 1.42 in.)
$I_{h\ell}$	flap system hinge line moment of inertia, determined with model assembled and including effective inertia of coil springs, kg–cm² (lb-in.-sec²)
K	rotary stiffness of coil-spring and flexure system, $(2\pi f_{no})^2 I_{h\ell}$, N–cm/rad (in.–lb/rad)
k	linear stiffness corresponding to K, $\dfrac{K}{h^2}$, N/cm (lb/in.)
k′	flap reduced frequency, $\dfrac{2\pi f_n (c/2)}{V_\infty}$
M_{nom}	nominal free-stream Mach number in tunnel
M_{meas}	measured free-stream Mach number in tunnel
p_ℓ	static pressure at lower model orifice, N/cm², abs (psia)
p_t	measured total pressure in transonic test, N/cm², abs (psia)
$p_{t_1 nom}$	nominal reservoir pressure in hypersonic test, N/cm² abs (psia)
p_{t_2}	calculated pitot pressure in hypersonic test, N/cm², abs (psia)
p_u	static pressure at upper model orifice, N/cm², abs (psia)
p_∞	calculated free-stream pressure in hypersonic test, N/cm², abs (psia); also measured free-stream pressure in transonic test, N/cm², abs (psia)
$\Delta p_{\ell rms}$	root mean square oscillatory pressure at lower model pressure cell, N/cm², abs (psia)
Δ_{urms}	root mean square oscillatory pressure at upper model pressure cell, N/cm², abs (psia)
q_∞	free-stream dynamic pressure, calculated, N/cm², abs (psia)
S	flap area (36.08 cm² or 5.592 in.²)
T_g	temperature at strain gage in hypersonic test, °K (°F)

T_ℓ	temperature at lower model thermocouple, °K (°F)
T_u	temperature at upper model thermocouple, °K (°F)
T_0	measured total temperature in hypersonic test, °K (°F)
$T_{0\,nom}$	nominal reservoir temperature in transonic test, °K (°F)
V_∞	free-stream flow velocity, m/sec (ft/sec)
α_{meas}	measured model angle of attack, rad (deg)
α_{nom}	nominal model angle of attack, rad (deg)
δ_f	flap mean angle, rad (deg) ($\delta_f = 0$ when flap flush with body)
$\Delta\delta_{frms}$	root mean square flap rotational oscillation
ζ_{01}, ζ_1 ζ_2, ζ_3	damping ratios in analog simulation
ζ_f	flap damping ratio (ratio of actual damping to critical damping)
ζ_{fs}	flap damping ratio in still air

HYPERSONIC AND TRANSONIC BUZZ MEASUREMENTS ON THE

LOWER PITCH FLAP OF THE M2–F2

LIFTING ENTRY CONFIGURATION

Robert W. Warner and Phillip R. Wilcox

Ames Research Center

SUMMARY

Free-oscillation damping measurements at hypersonic and transonic Mach numbers are presented for the lower pitch flap of a wind-tunnel model of the M2–F2 reentry vehicle. For the hypersonic test, the nominal Mach number is 7.3, the Reynolds number (based on 30.5 cm (1 ft)) ranges from 0.257×10^6 to 4.66×10^6, the angle of attack ranges from -0.105 rad (-6°) to +0.349 rad (+20°), and the mean flap deflections are 0.611 rad (35°) and 1.047 rad (60°) down from the local body contour. For the transonic test the mean flap deflection is 0.611 rad (35°), the Mach number ranges from 0.85 to 0.99, the Reynolds number (with length as above) from 4.35×10^6 to 4.97×10^6, and the angle of attack from -0.068 rad (-4°) to +0.244 rad (+14°). For the flow and model conditions tested, the damping measurements (together with flow pictures and pressure information) indicate the absence of hypersonic buzz instability for flap rotation frequencies of 47.3 Hz, 153 Hz, and 360 Hz, the presence of transonic buzz for the 47.3 Hz flap, and the absence of transonic buzz for a 115 Hz flap (all with a flap chord length of 4.384 cm (1.726 in.)). There is not enough flap damping data for an error estimate based on repeatability, but a partial damping calibration is presented in which an analog computer simulation of the random flap response for a known flap damping is fed into the autocorrelation computer and filter combination used for most of the damping measurements.

INTRODUCTION

Shock waves and the boundary layer provide a possible mechanism for hypersonic buzz instability of aerodynamic control surfaces, such as those to be used on space shuttle vehicles; and transonic buzz is an established phenomenon for airplanes. These issues have been investigated for the control flaps of several lifting entry configurations (refs. 1, 2, and 3). (Reference 4 is a study that came to the author's attention as this report was being prepared for publication.) A conservative design criterion is given for transonic buzz in reference 5. Actual aerodynamic damping has not been measured for the flaps in references 1, 2, and 3, however. Thus the designer is required, in the absence of a validated buzz theory, to account for oscillatory pressures due to flap vibrations by adopting a conservative and overly heavy configuration. In addition, the M2–F2 lifting body configuration, investigated statically in reference 6, has not been tested for buzz. The purpose of this study has been to measure damping hinge moments for the lower pitch flap of the M2–F2 and thereby, with the aid of flow pictures and pressure information, determine whether the model tested is subject to hypersonic or transonic buzz.

TEST EQUIPMENT AND PROCEDURE

Component parts of the M2–F2 reentry body model are shown in figure 1, a block diagram for the data recording and monitoring in figure 2, the model installation in the 3.5–foot hypersonic wind tunnel in figure 3, the installation in the 6– by 6–foot supersonic wind tunnel in figure 4, a block diagram for the data reduction in figure 5, a sample unfiltered spectrum in figure 6, and a preliminary damping calibration by analog simulation in figure 7.

Model

The model (fig. 1) has an overall length of 33.8 cm (13.3 in.) from nose to boattail, and was made by modifying the existing M2–F2 model (without canopy attachment) of reference 6 for flap buzz testing. The fixed lower pitch flap was replaced by a flap block that rotated about a hinge flexure. The hinge flexure was attached by placing its tapered end fittings in tapered cavities gouged in both the model body and the flap block and then pulling taper blocks in adjacent to the fittings by means of threaded drive bolts (details in figs. 1(b), (d), and (e)). This attachment technique, together with the requirement that bolts be loaded almost exclusively in tension throughout the system, resulted in a low system structural damping (damping ratio somewhat lower than 0.001 in some cases) and thereby facilitated the measurement of the additive aerodynamic damping.

Two flap blocks were used at hypersonic Mach numbers, one with a 1.047 rad (60°) and the other with a 0.611 rad (35°) mean flap angle (measured downward from the local body contour). The 1.047 rad (60°) angle is close to the angle required for trimmed zero lift (α = -0.122 rad (-7°)) and the 0.611 rad (35°) angle to that for trimmed $(L/D)_{max}$ (α = +0.209 rad (+12°)) at Mach numbers from 5.2 to 10.4 (ref. 6). In the transonic test, only the 0.611 rad (35°) flap block was used since that angle is close to the maximum required for transonic trim (α from -0.105 rad (-6°) to +0.349 rad (+20°) depending on upper flap position). For both flap blocks, the flap chord (c) was 4.384 cm (1.726 in.), and the flap area (S) was 36.077 cm² (5.592 in.²). The flap natural frequency was varied with the aid of four coil springs as shown in figure 1(c). (See appendix A for additional model information.)

APPARATUS AND INSTRUMENTATION

The Ames 3.5–Foot Hypersonic Wind Tunnel and 6– by 6–Foot Supersonic Wind Tunnel were used in these tests. Model installations are shown in figures 3 and 4, respectively. The hypersonic tunnel is a blowdown type having several interchangeable nozzles. The nozzle used in this test gives a nominal Mach number of 7.3 in the test section. The supersonic tunnel is a closed circuit, variable-density type with the floor and ceiling perforated to permit testing at transonic Mach numbers. The range in this test was from 0.85 to 0.99.

Another important piece of test apparatus was the trip mechanism (figs. 1(a), (b), and (f)). It engaged the trip stud on the flap along the center line of the coil spring. the engaging stroke in figure 1(f) being from BB to AA for the press-fit pin and from C to F for the slip-fit pin. When the hydraulic cylinder (2.86 cm (1–1/8 in.) stroke) was returned to its original position, the trip first rotated up to impart a step release for the flap and then returned along the slots AA–BB and A–C.

2

The end of the trip and also the trip stud were impregnated with permanent lubrication to reduce rubbing friction and thereby reduce vertical flap motion. High-speed movies indicated very nearly pure rotation of the flap after a trip.

The flap oscillations (from which were derived the flap damping ratio, ζ_f, the flap natural frequency, f_n, and the root mean square flap rotational oscillation, $\Delta\delta_{frms}$) were sensed by a four-strain-gage bridge (350 ohms per gage, good to $588.7°$ K ($600°$ F) on top of the hinge flexure and a similar bridge underneath. Calibrations were performed for the two softest flap systems by using a protractor to measure the change in flap angle when the trip mechanism was engaged and released. For the two stiffest systems, a similar calibration was performed with the coil springs removed and with flap-angle changes produced manually (since the trip thrust was insufficient for the two stiffest springs). When random oscillations made tripped decays useless, ζ_f and f_n were calculated by a correlation computer (ref. 7).

In addition to flap oscillations, the model measurements sought for both tests included root mean square oscillatory pressure (Δp_{urms}), static pressure (p_u), and temperature (T_u) on top of the model nose, together with similar quantities ($\Delta p_{\ell rms}$, p_ℓ, and T_ℓ) just upstream of the flap (precise locations in fig. 1(b)). The strain-gage temperature (T_g) was measured in the hypersonic test. Shadowgraphs were provided in the hypersonic test and Schlieren movies in the transonic test. Additional information can be found in appendix B.

TEST PROCEDURE AND DATA REDUCTION

The following data were obtained when needed just prior to a run or after a run, or both: flap hinge-line moment of inertia ($I_{h\ell}$), electrical and physical calibrations, still-air flap damping, and natural frequency.

The Reynolds number in the hypersonic test (M_{nom} = 7.3) ranged from 0.257×10^6 at p_{t_1} = 68.9 N/cm² abs (100 psia) to 4.66×10^6 at p_{t_1} = 1241 N/cm², abs (1800 psia) for the nominal reservoir temperature of $1055°$ K ($1440°$ F) and length of 30.5 cm (1 ft). (See chart 25 in ref. 8, with caloric corrections in charts 9 and 11, and a 3 percent reduction due to viscosity correction.) The selected angles of attack were +0, +0.105, +0.227, and +0.349 rad ($+0°$, $+6°$, $+13°$, and $+20°$) for all combinations of δ_f and f_{no} except δ_f = 1.047 rad ($60°$) with f_{no} = 47.3 Hz, for which α = -0 is added, and δ_f = 1.047 rad ($60°$) with f_{no} = 153 Hz, for which α = -0.105, -0, +0, +0.105 rad ($-6°$, $-0°$, $+0°$, $+6°$). The flap faces the tunnel wall supporting the quick insert strut at negative angles of attack and faces the other wall at positive angles.

For the transonic continuous-flow tunnel operation, various Mach numbers and angles of attack were surveyed in search of instability before data were taken. The nominal angle of attack ranged from 0 to +0.209 rad ($0°$ to $+12°$) for the 47.3 Hz flap and from -0.070 to +0.244 rad ($-4°$ to $+14°$) for the 115 Hz flap. The free-stream Mach number varied from 0.85 to 0.99 and the Reynolds number from 4.35×10^6 to 4.97×10^6 for a length of 30.5 cm (1 ft) with p_t around 10.3 to 11.7 N/cm², abs (15 to 17 psia) and with T_0 = $310.9°$ K ($100°$ F). Additional information on the test procedure is given in appendix C.

The instrumentation used for data reduction (block diagram in fig. 5, with measured quantities listed in the final blocks) was fairly typical except for the correlation computer mentioned earlier (ref. 7). An IBM 7094 program was used to curve fit the decays from the computer by least squares (ref. 9). The band-pass filter between the tape recorder and the computer was a Kron-Hite Model 3342 (with eighth order Butterworth used for both high and low pass) used to filter out unwanted modal frequencies (with a sample unfiltered spectrum shown in fig. 6).

Unfortunate consequences of the filtering were the requirements for a damping calibration and an estimate of the optimum filter setting. These requirements resulted from large variations in the apparent flap damping ratio when the filter pass band was broadened or narrowed around the frequency of flap rotation. The calibration and estimate were accomplished by analog computer simulation of the flap, its neighboring modes, and its random excitation in the wind tunnel; by feeding the taped random output of the analog into the autocorrelation computer with various filter settings; and by comparing the flap damping measured with the known damping from the analog. Details are given in appendix D.

RESULTS AND DISCUSSION

Test Results

Reduced numerical results for the hypersonic test appear in table 1 and for the transonic test, in table 2. Data time histories for certain cases of interest are shown in figure 8, selected damping results for the hypersonic and tansonic tests in figures 9 and 10, respectively, shadowgraphs for high and low flap damping at hypersonic speed in figure 11, and Schlieren movie frames for high and low flap damping at transonic speed in figure 12.

Discussion of Results and Unresolved Questions

The most important results of this investigation are the selected damping results of figures 9 and 10 (with the selections for the hypersonic test described in appendix E). Frequencies (f_n) are given in the legends either as discrete values (fig. 9(a)) or as ranges (fig. 9(c)). The data points are generally connected by straight lines to help identify trends. The ranges in f_n are more probably due to model assembly than to unsteady aerodynamics (slight variations in the parallel between hinge and spring flexures are possible between runs and even during a run). The larger range of f_n in figure 9(d) may result from the presence of more than one mode. For each plotted point in figures 9 and 10, the high and low pass filters are both set at the value of f_n (the actual values being given in tables 1 and 2 if not in figures 9 and 10).

Hypersonic buzz investigation for 47.3 Hz flaps— Hypersonic buzz is suspected when a flap damping value (ζ_f) is in or below the still-air band (ζ_{fs}). This implied subtraction of ζ_{fs} from ζ_f to get the aerodynamic damping is justified because the flap-spring combination is too massive to permit the air flow to affect the natural frequency.

For reservoir pressures ($p_{t1\,nom}$) below 345 N/cm², abs (500 psia) in figures 9(a) ($\delta_f = 0.611$ rad (35°)) and 9(c) ($\delta_f = 1.047$ rad (60°)), the damping values lie almost entirely within

the still-air damping bands, where both wind-on and still-air values are determined by oscillograph decays with the trip mechanism. Since there is no variation of ζ_f with nominal model angle of attack (α_{nom}) for these lower pressures, it is likely that the pressures are simply not large enough to affect the flap and that the damping values are essentially still-air magnitudes.

At 689 N/cm² abs (1000 psia), however, there is a definite trend toward low damping and possible buzz as the angle of attack decreases toward zero (supported somewhat by a similar trend in fig. 9(d) for a stiffer model at 345 N/cm², abs (500 psia)). In figure 9(c) this trend (at 689 N/cm², abs (1000 psia)) is for a curve in which the gap at the flap hinge line was covered by silicone rubber for all points. (Note that these damping results were measured by the correlator because the random oscillations were too large for oscillograph decays to be decipherable.)

In figure 9(a), this damping trend leads to a value at $\alpha = 0°$, below the still-air band. It is also below the still-air values for that particular run and the time-adjacent runs (items 1, 14, and 16 in table 1(a)) that were rejected for the still-air band as stated in appendix E. In fact, the damping value of 0.0006 for item 2 in table 1(a) is low enough so that the consistent filter and correlator errors discussed earlier will make the corrected damping value still lower (fig. 7). A further suggestion of possible buzz is the root mean square oscillatory pressure ($\Delta p_{\ell rms}$) for item 2, which (if assumed uniformly distributed over the flap area with the proper phase in harmonic motion) is almost four times larger than that required to cancel the still-air damping moment based on ζ_{fs} in item 1.

Despite the above evidence of buzz for item 2 in table 1(a) and figure 9(a), the damping value of 0.0006 is considered more likely to be an essentially still-air phenomenon than a buzz phenomenon. The measured p_ℓ somewhat upstream of the flap, as recorded in table 1(a), is low enough to enhance the possibility of still-air vibrations, particularly at a zero angle of attack (item 2). The strongest indication of still-air vibrations, however, results from examination of the shadowgraphs.

Figure 11(a) is a shadowgraph picture corresponding to item 3 in table 1(b) with $f_{no} = 360$ Hz and hence, for static purposes, to item 2 in table 1(a) with $f_{no} = 47.3$ Hz, for which no shadowgraph is available. Figures 11(b) and (c) are shadowgraphs corresponding to item 17 in table 1(b) and item 30 in table 1(a), respectively, with both included to illustrate the lack of frequency effect on the static shock and separation pattern.

Inspection of these shadowgraphs shows that the low damping case (item 2 in table 1(a), $\alpha_{nom} = 0$) has no significant shock or separation around the flap (fig. 11(a)) while the high damping case (item 30 in table 1(a), $\alpha_{nom} = 20°$) has both (fig. 11(b) or (c)). The reverse should be true if the shock and separation were producing buzz by means of appropriately phased signaling between the flap and the weak shock at the separation point upstream. This indicates that the potential buzz mechanism is producing damping (stabilizing) rather than fanning (destabilizing) as α_{nom} increases and that the low damping of item 2 in table 1(a) and figure 9(a) is essentially still-air damping.

The remaining value of $p_{t_1 nom}$ to be considered is 345 N/cm², abs (500 psia) in figure 9(a), for which a damping value is given only at $\alpha_{nom} = 0°$. Since this value of $p_{t_1 nom}$ lies between the two reservoir pressures already discussed, it is concluded that its low damping value simply means effective still-air damping and not buzz.

Hypersonic buzz investigation for 153 Hz and 360 Hz flaps— The most believable low damping values (wind-on) in table 1(d) and figures 9(b) and (d) occur at $\alpha_{nom} = 0$ or $\alpha_{nom} = -0.105$ rad (-6°), as noted in appendix E. These are regarded as effective still-air values for the same reasons given for the 47.3 Hz flaps.

Thus, hypersonic buzz is considered absent for the various model M2—F2 lifting body configurations and flow conditions tested in the present project. It was also considered absent for the model vehicle configurations of reference 2.

Transonic buzz investigation for 47.3 Hz flap— For the transonic test, the damping plots (fig. 10) have Mach number as the parameter instead of tunnel reservoir pressure (total pressure being held close to atmospheric pressure for the transonic test). The only static flap angle (δ_f) tested was 0.611 rad (35°). For the 47.3 Hz flap, figure 10(a) includes all damping values from table 2(a) except that for item 9. This item is rejected because its time history is nonlinear as seen in figure 8(c) due to gage malfunction. Item 12 has no damping value in table 2(a) because its time history appears to be nonstationary, as suggested by the erratic shifting of the oscillation mean line in figure 8(d).

An acceptable unfiltered time history for the correlation computer is shown in figure 8(e) for item 8 in table 2(a). Actually, the strain gage had malfunctioned earlier for magnitude purposes (because of large oscillations). The latest correlate (i.e., highest numbered correlate) for which $\Delta\delta_{frms}$ could safely be given was correlate 46 (item 3), but the correlation computer can be believed as long as the time history is linear and stationary.

For M = 0.90 there is an erratic trend toward low damping and possible buzz as the angle of attack increases toward +0.209 rad (+12°). Another possible buzz point with damping below the still-air value is the point at $\alpha = 0.105$ rad (+6°) for M = 0.95 (item 10 in table 2(a)), but there are not enough points to establish a trend for this Mach number. Both of the possible flutter points just mentioned have damping values low enough so that they will be still lower when corrected for consistent filter and correlator errors (fig. 7), and item 10 is the point for which the damping calibration particularly applies (see appendix D).

In contrast to the possible hypersonic buzz conditions discussed earlier, the two possible transonic buzz points in figure 10(a) are considered to be actual buzz rather than effectively equal to still-air vibrations. The likelihood of effective still-air vibrations is reduced relative to the hypersonic test because the static pressures somewhat upstream of the flap are much higher in table 2 than in table 1.

Another reason for considering the possible buzz to be actual buzz in the transonic test is the presence (in contrast to the hypersonic test) of the potential buzz mechanism at the possible buzz points as well as the high-damping points. Thus, the shock upstream of the flap is present in the Schlieren movie frames of figures 12(a) and (c). In addition, the data of figure 10(a) are supported as buzz data by the fact that the corresponding still-air damping (1) was reduced exclusively by oscillograph decay, (2) had very little variation during the decay (item 1 in table 2(a)), (3) had a low enough value so that major reduction by model shakedown would not be expected, and (4) was not subjected to large temperature variations during the test. Finally and most importantly, the existence of transonic buzz is supported by the visual observation of flap oscillations considerably larger than the $\Delta\delta_{frms}$ values reported in table 2(a).

Transonic buzz investigation for 115 Hz flap– For the 115 Hz flap, figure 10(b) includes all damping values from table 2(b) except those for items 5, 7, 9, 11, 13, and 15. These were excluded because the trip mechanism used during data taking might possibly cause a large error in the data reduction by the correlation computer (which had to be used because the random oscillations made the decays undecipherable). Actually, these data might have been included in figure 10(b), except for consistency with the hypersonic test, since the trip did not cause the large reduction in apparent damping noticed in the hypersonic test (possibly because the ratio of trip amplitude to rms random amplitude was relatively smaller for the transonic test or possibly because of differences in trip amplitude and model frequency). In fact, in the transonic test, the correlation computer data with and without trips agree remarkably well with each other and display no consistency as to which is higher, yielding evidence of good repeatability.

Because of this repeatability, together with damping values that were high enough to minimize filter and correlator errors, the data of figure 10(b) are considered to be the best reported here. In fact, the data points for various Mach numbers lend themselves to a possible data band, as shown shaded in figure 10(b). This data band indicates the absence of buzz for the α and M values plotted a result considered valid despite the potential buzz mechanism implied by the shock in figure 12(d).

Thus, transonic buzz was present for the 47.3 Hz system and absent for the 115 Hz system. This parallels the results of reference 3 for a different entry configuration. It is worth noting that the reduced frequency $(k' = [2\pi f_n(c/2)]/V_\infty$ are roughly 0.02 and 0.05 for the 47.3 and 115 Hz systems, respectively. These are well within the region $(k' < 0.3)$ in which proof tests are recommended for transonic buzz in reference 5.

Reliability of damping measurements– No quantitative error estimate can be made for the damping measurements that have just been discussed. To do so would require repeatability checks within the calibration scheme or for tests in a given wind tunnel, repeatability checks from tunnel to tunnel, repeatability checks from method to method (an alternate method being harmonic oscillation at resonance, refs. 10 and 11), and additional calibrations.

Thus, the damping plots in figures 9 and 10 indicate trends but are questionable for damping magnitudes, particularly when the damping is low or when spurious modes are present. Except for figure 10(b) $(f_{no} = 115$ Hz, transonic flow), all of the parts of figures 9 and 10 are considered to require additional information (such as flow pictures, pressure distributions, and observations of large oscillations) before a conclusion can be drawn on the presence or absence of buzz.

It should also be stated, however, that there are no quantitative damping measurements in references 1, 2, and 3 and that error estimates on damping measurements for rough flow in a wind tunnel have not been found in the literature. Reference 12 gives an error estimate for damping $(C_{mq} + C_{m\dot{\alpha}})$ for vehicles having smooth flow. For a specific vehicle having rough flow, however, reference 12 states that an error estimate cannot be made because of large differences between vehicle damping values measured in different wind tunnels (such as $C_{mq} + C_{m\dot{\alpha}} = +0.15$ in one tunnel and -0.25 in another). The measurement of damping for rough flow in a wind tunnel is apparently a difficult subject that has received little attention.

Qualitative discussion of possible errors– In addition to the error sources already discussed, a number of possible (but probably less harmful) error sources remain. Attention is restricted to the

damping measurements, and no attempt has been made as yet to correlate such quantities as the various thermocouple readings before a run (with the model possibly still hot from a previous run).

The error magnification due to subtraction of the still-air damping values in figures 9 and 10 from the largest total damping values appears to be trivial. If this subtraction were actually carried out some of the error due to spurious modes would be removed, particularly when the flap rotation frequency is the lowest of those present.

Although the correlator results with the longest record time and the most correlates are the most believable in tables 1 and 2 (when all else is equal), there were always enough correlates for convergence. The time histories and the Beckman readouts suggested some error due to variable tunnel conditions, but all cases with large variations were deleted. The Mach number and stream angle variations reported earlier should not introduce significant errors.

In the transonic test, however, the Mach numbers reported as 0.95 and 0.99 might not be precise. For example, the measured Mach numbers in table 2 are often a little above 1.00, but in that range a tunnel normal-shock wave was just upstream of the model. Tunnel resonance frequencies and compressor blade frequencies (ref. 13) could conceivably affect dynamic measurements in the transonic test but should be minimized by viscous effects. Resonance, in particular, should be minimized by the small model size relative to the wind tunnel.

Possible additional applications of present data— The ζ_f in tables 1 and 2 and figures 9 and 10 can be expressed as dynamic-stability type hinge-moment coefficients by the equation

$$C_{h\dot{\delta}_1} = -\zeta_f \left[\frac{2I_{h\ell}(2\pi f_n)V_\infty}{q_\infty Sc^2} \right]$$

where

$$\dot{\delta}_1 = \frac{\dot{\delta}c}{(12)V_\infty}$$

The moments of inertia $I_{h\ell}$ can be found in figure 1(d); c = 4.384 cm (1.726 in.); S = 36.07 cm² (5.592 in.²); $\dot{\delta}_1$ is the flap rotational velocity in rad/sec; and f_n, V_∞, and q_∞ can be found in, or calculated from, tables 1 and 2. For conversion to flutter-type hinge-moment coefficients, the following equation can be used.

$$C_{h\delta I} = -\zeta_f \left[\frac{2I_{h\ell}(2\pi f_n)^2}{q_\infty Sc} \right]$$

The subtraction of still-air damping from flow damping can be done before or after conversion to $C_{h\dot{\delta}1}$ or $C_{h\delta I}$ since the air flow cannot significantly affect the natural frequency of the massive flap-spring system.

A more important additional application of the present data is the determination of the input spectral density for the flap. The rms output is given in tables 1 and 2 for certain cases; and the transfer-function quantities, ζ_f and f_n, are the principal results of this investigation. With these, the input spectral density is given by equation (9) of reference 7 for isotropic turbulence with a known cutoff frequency, ω_1. How much of the input is buffet and how much is tunnel roughness must still be determined.

Unresolved questions— The results and potential errors discussed qualitatively so far pertain only to the present model in the present tests. The possibility of generalizing the results to flight configurations leads to a number of unresolved questions. For example, the effects of different model supports, various rudder positions, the presence and position of upper flaps, decreased lower flap angles, boundary layer trips, Reynolds number changes without density changes, various oscillation amplitudes, and a more realistic shape for the leeward side of the model flap — all these remain unknown (the minimal investigation of two sting lengths and two model positions relative to the quick insert strut in the hypersonic test (fig. 9(d)), as well as the oil flow studies, being inconclusive at the present time).

The unknowns just listed would make questionable the application of these results to an M2–F2 flight vehicle, let alone to a different body shape. It is therefore clearly desirable to use these and previous results in attempting to formulate a semiempirical buzz theory employing measured (or otherwise estimated) static pressures and temperatures. Such a theory should have broad applicability to airplanes and space shuttle vehicles as well as lifting bodies.

CONCLUSIONS

An experimental investigation of damping hinge moments for the lower pitch flap of the M2–F2 lifting body entry configuration has been carried out in the Ames 3.5–Foot Hypersonic Wind Tunnel at a nominal Mach number of 7.3 and in the Ames 6– by 6–Foot Supersonic Wind Tunnel at transonic Mach numbers. The same model was used in both tests, with the flap undergoing random aerodynamic excitation and tripped free decays. The unavoidable random excitation made the free decays undecipherable except at the lowest tunnel reservoir pressures in the hypersonic test, where the effect of the airstream on the flap damping was apparently negligible. The most useful measurements, then, of aerodynamic plus structural damping of the lower pitch flap were made by computing the autocorrelation function of the random response.

Unfortunately, several modes were present in the random response, in addition to the flap rotation mode. Hence, filtering was required, together with the determination of an optimum filter setting and a possible calibration factor. This was accomplished, in part, by analog computer simulation of the random flap response and by comparing the assigned flap damping with that read by the autocorrelation computer and filter combination from the analog tape.

No quantitative error estimate can be made on the basis of repeatability. To do so would require much additional research. On the basis of the results obtained, however, the following conclusions are offered for the configuration tested, which has a flap chord length of 4.384 cm (1.726 in.).

1. There is no hypersonic buzz instability at a Mach number of 7.3 for flap rotation frequencies of 47.3 Hz, 153 Hz, and 360 Hz. The low flap damping measured at low angles of attack is accompanied by low flap pressures and is considered to be essentially a still-air phenomenon.

2. Transonic buzz is present for the 47.3 Hz flap and absent for a 115 Hz flap.

Ames Research Center
   National Aeronautics and Space Administration
      Moffett Field, California, 94035, October 13, 1971

APPENDIX A

ADDITIONAL MODEL INFORMATION

The hinge flexure (fig. 1(e)) was placed slightly inside the bottom contour of the body to protect the strain gages from the high stagnation temperature in the 3.5−foot hypersonic wind tunnel. The resulting gap at the flap root was occasionally covered with silicone rubber to keep the hot air from being sucked in around the gages. In the 6− by 6−foot supersonic wind tunnel, the silicone rubber was not needed. Except for this difference and the selection of mean flap angles and coil springs, the model was identical for the tests in the two wind tunnels.

For all flap angles, the flap block extended upward from the flap area through a large cut in the removable boattail and was attached to a large coil spring by means of a "spring flexure." The spring flexure (figs. 1(b) and (c)) was parallel to the hinge flexure and was located 3.61 cm (1.42 in.) above it. Four coil springs were used to give four flap frequencies for various phases of the test program, with spring dimensions given in a table in figure 1(c) and with dimensions for the corresponding spring flexures and hinge flexures given in figures 1(c) and (e), respectively. The coil spring deflections that produced a total strain of 0.001 (fatigue endurance limit) in the corresponding hinge and spring flexures were 0.160, 0.079, 0.079, and 0.041 cm (1/16, 1/32, 1/32, and 1/64 in.) for the successively stiffer coil springs. The corresponding flap angle increments were 0.044, 0.022, 0.022, and 0.011 rad (2.52°, 1.26°, 1.26°, and 0.63°), respectively.

The system frequencies (f_{no}) given in figures 1(c), (d), and (e) were the frequencies of the flap-spring system most representative of the still-air data, 47, 3, 115, 153, and 360 Hz. The flap system hinge-line moments of inertia ($I_{h\ell}$) in figure 4(d) were found immediately before (or sometimes after) each model configuration was used for the first time by measuring the frequencies that resulted from known additions of inertia, which permitted calculation of the basic flap system inertia (a broken strain gage prevented the inclusion in figure 1(d) of an inertia value for f_{no} = 153 Hz, δ_f = 1.047 rad). These flap system inertia values included the effective inertias of the coil springs and all other moving parts. The corresponding spring stiffness (k) in figures 1(c), (d), and (e) were calculated on the basis of f_{no} and $I_{h\ell}$. There were some variations from the representative values of f_{no} and k, probably associated with such problems as the assembly of the spring and hinge flexures slightly out of parallel.

11

APPENDIX B

ADDITIONAL INFORMATION ON APPARATUS AND INSTRUMENTATION

The M2–F2 model for flap buzz was first installed on the quick insert mechanism in the Ames 3.5–Foot Hypersonic Wind Tunnel (fig. 3). This mechanism allows the model to be injected and withdrawn rapidly when desired (which permits still-air damping measurements during or immediately after a run if temperature variations are important). For the Mach 7.3 nozzle of the hypersonic wind tunnel, unpublished work of Thomas E. Polek indicates the maximum Mach number variation at the model location (but without the model) to be 0.04 over the model length and 0.10 in the radial direction from the sting axis. The same work shows the maximum flow-angle corrections for a model at roughly the same location to be -0.004 rad (-0.26°) in angle of attack and -0.001 rad (-0.06°) in yaw.

In a later test at transonic Mach numbers, the model was installed in the Ames 6– by 6–Foot Supersonic Wind Tunnel (fig. 4). At these Mach numbers, unpublished work of John W. Boyd shows the axial Mach number variation along the tunnel center line to be no more than ±0.01 from the average free stream Mach number. At the model location, the maximum vertical deviation was also approximately ±0.01. The same work shows the correction in angle of attack to be roughly -0.003 rad (-1/6°) at the model location in the Mach number range from 0.880 to 0.979. With respect to flow pressure fluctuations at the same location, unpublished work of Jules B. Dods, Jr., gives the following table for a total head of 6.78 N/cm² (9.83 psi):

Mach number	$C_p = \dfrac{\text{rms pressure fluctuation}}{\text{free-stream dynamic pressure}}$	Free stream dynamic pressure, N/cm² (psi)	$\dfrac{\text{rms pressure fluctuation}}{\text{free-stream static pressure}}$
0.80	0.01397	1.98 (2.87)	0.0063
.94	.00787	2.34 (3.40)	.0049

The rms pressure fluctuations on the model, $\Delta p_{u_{rms}}$ and $\Delta p_{\ell_{rms}}$ were measured by Schaevitz-Bytrex HFD–HT2 pressure transducers (good to 533.2° K (500° F), ±1.38 N/cm³ (±2 psi)) in the hypersonic test and by HFD–2 transducers (good to 422° K (300° F), capacity ±1.38 N/cm² (±2 psi)) in the transonic test, with calibrations applied by a static pressure calibrator at 0 and 0.17 N/cm² (0.25 psi). The static pressures p_u and p_ℓ were measured by Statham pressure cells of 3.45 N/cm² (5 psi) capacity in the hypersonic test and 10.3 N/cm² (15 psi) capacity in the transonic test, with several manometer calibration points per cell. The temperatures T_u and T_ℓ were measured by chromel-constantan thermocouples, insulated from the model by ceramic, with a 338.7° K (150° F) reference box and accompanying temperature-millivolt table. The same system was used for T_g but without insulation.

In the hypersonic test, nominal tunnel temperatures and pressures specified for the tunnel operation were considered to be sufficiently accurate, except that an average of the measured reservoir temperatures was used instead of nominal values. For the transonic test, the local total head (p_t) and the local tunnel static pressure (p_∞) were measured by tunnel cells, the tunnel stagnation temperature (T_0) by a tunnel thermocouple, and the model angle of attack (α_{meas}) by a tunnel pickup. Beckman equipment was used for the quantitative recording of these parameters.

Beckman equipment was also used for the quantitative recording of the model parameters p_u, p_ϱ, T_u, and T_ϱ in the transonic test and p_u and p_ϱ in the hypersonic test.

The instrumentation chain of figure 2 was used in both tests for the qualitative monitoring of any rapid fluctuations in tunnel and model parameters as functions of time and also for the quantitative recording and monitoring of flap and pressure oscillations. The chain was fairly typical except for the correlation computer (ref. 7). Since more than one degree of freedom was present, a band-pass filter was useful with the computer for monitoring ζ_f during the test. The oscillograph was used to monitor oscillation amplitudes. The Brown recorders were used to monitor model temperature during the hypersonic test only.

APPENDIX C

ADDITIONAL INFORMATION ON TEST PROCEDURE

For the two softest systems (f_{no} = 47.3 Hz and 115 Hz), the most important steps in the model assembly prior to a run were to shim the coil spring for the desired neutral flap position, under the estimated static aerodynamic hinge moment, and to shim the trip stud (if tripping was used) for the desired trip amplitude. (Tripping was impossible and static flap rotations insignificant for the two stiffest springs.)

During tunnel operation in the hypersonic and the transonic tests, an attempt was made to provide data time for random oscillations equal to at least 10 times the reciprocal of the bandwidth for a flap damping ratio of 0.001 ($t_{record} = (10/2\zeta_f f_{no}) = (5,000/f_{no})$). As seen in table 2, this data time was achieved in the transonic test for each Mach number and angle of attack with time left over for tripped oscillations (if any). In the hypersonic test, table 1 shows that this data time was almost always achieved for each reservoir pressure and angle of attack with f_{no} = 360 Hz, rarely achieved with f_{no} = 47.3 Hz, and achieved half the time with f_{no} = 153 Hz. The desired data time is not considered an absolute requirement for good data, but the data having the shortest time for a given ζ_f and f_{no} is considered the least reliable, all other things being equal.

For the hypersonic blowdown tunnel operation, the Mach number of roughly 7.3 was developed and stabilized at the desired reservoir pressure before the model was inserted into the tunnel (the model generally having been sprayed with sensitive paint for temperature studies or dotted with titanium oxide and oil for flow studies). After a prescribed time for data taking, $p_{t1\,nom}$ was changed for further data taking when time allowed. When the final value of $p_{t1\,nom}$ could no longer be maintained, the model was retracted.

A number of the earliest runs in the hypersonic test were devoted to a temperature survey with no strain gage or pressure cells. These delicate transducers were installed only when the temperature distributions were known.

14

APPENDIX D

PARTIAL CALIBRATION FOR DAMPING AND ESTIMATE

OF OPTIMUM FILTER SETTING

In an attempt to determine an optimum filter setting and a possible damping calibration factor for the random data, three linear and uncoupled modal degrees of freedom with constant coefficients were set up on an analog computer. Decay records were taken on magnetic tape so that the input damping ratios and natural frequencies would be known regardless of analog computer error or drift. Immediately thereafter white noise was used to force the three degrees of freedom, and a weighted sum of their unfiltered analog responses was recorded on the same magnetic tape for two minutes. The weighting parameters and other system parameters had been selected earlier to approximate very roughly the unfiltered correlation function of a segment of taped experimental data (transonic).

Various band-pass filter settings were then applied to the analog tape to separate the degree of freedom having the flap frequency from the two neighboring degrees of freedom, and the filtered responses were fed into the correlation computer. The output damping measured on the computer for the flap (ζ_{01}) was divided by the known analog input damping (ζ_{i_1}), and figure 7 shows the resulting ratio (ζ_{01}/ζ_{i_1}) plotted against increasingly narrow band-pass filter settings. The desired ratio is unity, of course.

The numbers opposite the sample symbols in figure 7 are the known input damping coefficients (ζ_{i_1}, ζ_2, ζ_3) and natural frequencies (f_{n_1}, f_{n_2}, f_{n_3}) for the three degrees of freedom on the analog tape. Approximate values for f_{n_2} and f_{n_3} were determined by a qualitative spectrum analysis of the selected segment of taped experimental data without filtering (fig. 6). Improved values for ζ_2, f_{n_2}, ζ_3, and f_{n_3} were then determined by placing the center frequency of a band-pass filter near the sting mode and the unidentified mode (which may be flap vertical translation) in figure 6 and using the correlation computer to estimate frequencies and damping ratios. Final values for the data tape were determined by approximating the unfiltered data correlation function as mentioned earlier.

The flap input damping ratio (ζ_{i_1}) was selected as 0.001 for one case in figure 7 and 0.002 for a second case. These were useful and representative values, but the variable aerodynamic damping would require more cases for a complete calibration and determination of the optimum filter setting (also more data segments for more flap configurations, model angles of attack, Mach numbers, etc., with final calibration curves consisting of plots of the damping output-input ratio versus damping output at the optimum filter setting). An attractive alternative is to settle for a partial calibration in which only the points of greatest interest (lowest damping) are checked by the analog computer tape.

The present effort was limited to the two cases in figure 7 because of the large computer turn-around time in digitally curve fitting the decays from the correlator. For these two cases, the optimum filter setting clearly occurs (ζ_{01}/ζ_{02} nearest unity in fig. 7) when both filters in the band pass are set at the flap rotation frequency of 47.6 Hz (or near it); and all data reduction is performed with filtering at the flap frequency, regardless of its value.

The improvement of results in figure 7 as the filter band pass is narrowed suggests that insufficient filtering is a major cause of error among the possible causes listed earlier. A question arises, then, about why results for the lower damping get worse in figure 7 when the filters are crossed (to the right of 47.6–47.6 Hz) to give a partial band reject. The reason is probably the loss of signal that occurs with band reject.

Since ζ_{01}/ζ_{i_1} follows a consistent trend in figure 7, it can be regarded as a calibration (specifically, an "environmental calibration," which is taken here to mean a damping calibration applicable to the random flap oscillations in the wind tunnel). This partial calibration is based on wind tunnel data for item 10 of table 2(a) in the transonic test, and $\zeta_{i_1} = 0.001$ is the closest of the two calibration cases to $\zeta_f = 0.0005$. Item 10 is a point of great interest since $\zeta_f = 0.0005$ is lower than the still-air damping value $\zeta_{fs} = 0.0010$ in table 2(a). Such a partial calibration does not, of course, justify the application of a general correction factor from figure 7 to the whole body of damping data.

Despite the lack of a complete calibration, the error information remains useful for qualitative trends, particularly since ζ_{01}/ζ_{i_1} is always equal to or greater than unity in figure 7. In this sense, it is worth noting that the error at the optimum filter setting in figure 7 is close to zero for $\zeta_{i_1} = 0.002$ and ranges from 10 to 30 percent for $\zeta_{i_1} = 0.001$.

The reason for the error difference just noted is probably that computing errors can affect the lower damping values more than the higher ones (with the close filter spacing minimizing errors due to insufficient filtering and the low damping minimizing those due to filter transients). This suggests that higher still air damping values (with the resulting higher total damping values) would have reduced errors throughout the present tests, providing they were not too much higher. If the model flap had originally been intended for free random oscillation rather than forced harmonic oscillation, it would have had lower inertias and higher damping (percent critical).

The optimum filter setting estimated above for random data was also used for the relatively pure tripped decays (for which the setting may no longer be optimum). For an estimate of filter transient error (and possible calibration) with decays, the present eighth order Butterworth-type filters and the model flap were approximated by linear and second-order transfer functions with constant coefficients. The classical linear decay solution (for an initial flap displacement) of the resulting three-part chain of second-order systems was evaluated digitally at enough points in time to permit the filtered damping ratio to be calculated from cycle to cycle over 10 cycles.

In this solution, the buildup of the filtered response from zero initial conditions (for the high-pass filter) required two cycles for the assigned flap frequency and initial displacement (in contrast to fig. 8(a) for a different combination of frequency and displacement with the actual model and filters). Despite some persistence of damping error beyond the buildup, the filtered damping ratio after the third subsequent cycle differed from the assigned flap value of 0.001 by less than one part in 10,000. Hence the damping calibration factor for filter transients was taken to be unity for tripped decays.

APPENDIX E

SELECTION OF DAMPING RESULTS FOR FIGURE 9

Figure 9(a) specifically includes items 2, 10, 15, 17, 20, 25, 26, and 30 from table 1(a) for ζ_f and implicitly includes items 4, 9, 13, 19, and 24 in the ζ_{fs} band. Items 5, 6, 7, 11, 21, 22, 27, and 28 are rejected for ζ_f because the correlation computer often gives an unrealistically low estimate of flap damping when the trip mechanism is used. (The low correlator estimate results from the apparent rise of oscillation amplitude over several cycles because of filter response. The correlator was used instead of oscillograph decays because the residual random oscillations are large enough to affect the decays significantly — as seen in fig. 8(a) with filtering and fig. 8(b) without filtering for the first of four trips for item 28.) Items 8, 12, 23, and 29 are rejected for ζ_{fs} because the damping measurement may have been affected by a blast of cooling air in the jacket after the run (condition IAR in table 1(a)); and items 1, 3, 14, and 16 are rejected because oscillograph decays (OD) are considered better for still-air measurement than correlation results (CC) (because of the low level of random vibrations when the model is not in the tunnel air stream). Finally, item 18 is rejected for ζ_{fs} because this value is much higher than those for items 19 and 24 (all for the same run). (Possible reasons for this include temperature effects and the working into parallel of originally out-of-parallel hinge and spring flexures.)

For similar reasons, the only items from table 1(c) included in figure 9(c) are 1, 3, 6, 11, 12, 15, 26, 27, 32, and 35 for ζ_f and 10, 13, 14, 19, 21, 25, 28, 33, and 34 for the band of ζ_{fs}. A band was used for ζ_{fs} rather than individual data points to avoid cluttering the figures. This means, however, that a ζ_f value lying within the ζ_{fs} band may be above or below the ζ_{fs} values associated with its run or time-adjacent run.

For the stiffer configurations in the hypersonic test, all damping values from tables 1(b), (d), and (e) are used in figures 9(b) and (d), explicitly for the wind-on values and implicitly for the still-air bands. However, only items 3 and 9 in table 1(b), 3 and 6 in table 1(d), and 4 and 5 in table 1(e) had acceptable curve fits of the correlator decays by the least squares program for the damping values, with details given in the table footnotes. In addition, all still-air values for the stiffer configurations depended on the correlator using low-level random oscillations of the tunnel with the model in the jacket prior to insertion (condition IBR in table 2).

The results for the stiffer configurations are retained (marginally) only because the curve for the 345 N/cm² abs (500 psia) reservoir pressure ($P_{t1 \text{ nom}}$) in figure 9(d) follows the trend discussed earlier (with remarkable repeatability at $\alpha = 0.227$ rad (13°)) and because figures 9(b) and (d) are quite similar above $\alpha = 0.105$ rad (6°). With item 14 in figure 9(b) rejected as an obvious error (the correlator being unable to give a negative damping) and with item 5 in figure 9(d) rejected as a less obvious error (in the absence of a trend), the remaining low damping values (wind-on) occur at $\alpha_{\text{nom}} = 0°$ and $\alpha_{\text{nom}} = -0.105$ rad (-6°) in table 1(d) and at $\alpha = 0$ in figure 9(d).

REFERENCES

1. Goldman, R. L.; Morkovin, M. V.; and Schumacher, R. N.: Unsteady Control Surface Loads of Lifting Reentry Vehicles at Very High Speeds. AIAA J., vol. 6, no. 1, January 1968, pp. 44–50.

2. Goldman, Robert L.: Investigation of Control Surface Instability of Lifting Body Configurations. Tech. Report AFFDL–TR–65–106, Air Force Flight Dynamics Laboratory, 1965.

3. Goldman, Robert L.: Investigation of Transonic Control Surface Instabilities of a Lifting Body Configuration. Tech. Report AFFDL–TR–67–139, Air Force Flight Dynamics Laboratory, 1968.

4. Goetz, Robert C.; and Gibson, Frederick W.: Investigation of Control Surface Instabilities on Lifting-Body Reentry Vehicles at a Mach Number of 15.4. NASA TN D–6301, 1971.

5. Anon.: Flutter, Buzz, and Divergence. NASA SP–8003, 1964.

6. Axelson, John A.; and Mellenthin, Jack A.: Hypersonic Aerodynamic Characteristics of the M2–F2 Lifting Entry Configuration. NASA TM X–1690, 1968.

7. Cole, Henry A., Jr.: On-the-Line-Analysis of Random Vibrations. AIAA Paper 68–288, 1968.

8. Ames Research Staff: Equations, Tables, and Charts for Compressible Flow. NACA Rep. 1135, 1953.

9. Wilcox, Phillip R.; and Crawford, William L.: A Least Squares Method for the Reduction of Free-Oscillation Data. NASA TN D 4503, 1968.

10. Lessing, Henry C.; Fryer, Thomas B.; and Mead, Merrill H.: A System for Measuring the Dynamic Lateral Stability Derivatives in High-Speed Wind Tunnels. NACA TN 3348, 1954.

11. Beam, Benjamin H.: A Wind-Tunnel Test Technique for Measuring the Dynamic Rotary Stability Derivatives Including the Cross Derivatives at High Mach Numbers. NACA TN 3347, 1955.

12. Wehrend, William R., Jr.; and Reese, David E., Jr.: Wind-Tunnel Tests of the Static and Dynamic Stability Characteristics of Four Ballistic Reentry Bodies. NASA TM X- 369, 1960.

13. Molyneux, W. G.: Wind Tunnel Interference in Dynamic Measurements. Technical Report 64069, British Royal Aircraft Establishment, 1964.

TABLE 1.– HYPERSONIC TEST RESULTS AND DERIVED PARAMETERS
(M_{nom} = 7.3, V_∞ = 1353 m/sec,[a] $T_{0\,ave}$ = 962° K,[b] Δp_{urms} < 0.007 N/cm²[c])

(a) ζ_f = 0.611 rad, f_{no} = 47.3 Hz

Item	Condition[d]	Correlate number[e]	α_{nom}, rad[f]	$P_{t_1 nom}$, N/cm²[b]	f_n, Hz	ζ_f[g]	ζ_{fs}[g]	Damping measurement[h]	p_{t_2}, N/cm²[a]	p_∞, N/cm²[a]	q_∞, N/cm²[a]	p_u, N/cm²[i]	p_ℓ, N/cm²[i]	T_u, °K	T_ℓ, °K	T_g, °K	$\Delta\delta_{frms}$, rad[j]	$\Delta p_{\ell rms}$, N/cm²[j]	Trip used	Rubber used[k]	Correlation computer data time, sec[l]	Comments
1	IBR	171			47.6		0.0016	CC						329.3	347.6	344.3			No	No	55	
2	R(1)	171	0	689.5	47.6	0.0006		CC	8.281	0.1189	4.444	0.1689	0.1475	338.7	366.2	344.7	0.0843	0.0827	No	No	97	
3	OBR	64			47.6		.0017	CC						336.5	306.5				Yes	No	30	
4	IBR	67			47.6		.0016	OD						299.0	351.4				Yes	No		
5	R(1)	67	0	137.9	47.6	.0009		CC	1.655	.0238	.889	.0669	.0579	290.4	306.8	351.6			Yes	No	35	
6	R(2)	67	0	344.7	47.6	.0010		CC	4.139	.0594	2.222	.1007	.0772	302.3	317.6	298.4			Yes	No	37	
7	R(3)	67	0	689.5	47.6	.0008		CC	8.281	.1189	4.444	.1965	.1241	322.9	330.7	310.1			Yes	No	39	
8	IAR	67			47.6		.0016 to .0027	OD						335.7	331.2	312.9			Yes	No		
9	IBR	75			47.6		.0021 to .0027	OD							298.7	296.2			Yes	No		
10	R(1)	75	0	344.7	47.6	.0019 to .0030		OD	4.139	.0594	2.222	1103	0896		307.1	296.2			Yes	No		
11	R(2)	75	0	689.5	47.6	.0009		CC	8.281	.1189	4.444	2110	.1427		327.6	303.4			Yes	No	30	
12	IAR	75			47.6		.0017 to .0025	OD							335.4	325.1			Yes	No		
13	OAR	76			47.6		.0013 to .0015	OD							346.5	348.2			Yes	No		
14	IBR	174			47.6		.0016	CC						329.0	327.6	345.4			No	No	55	
15	R(1)	174	.105	689.5	47.6	.0016		CC	8.281	.1189	4.444	.1531	2358	335.1	367.3	346.5	.0885	.0869	No	No	107	
16	IBR	168			47.6		.0268	CC						327.6	346.2	343.6			No	Yes	50	
17	R(1)	168	.105	689.5	47.6	.0059		CC	8.281	.1189	4.444	1565	2386	339.8	399.8	343.8	.0892	.0876	No	Yes	105	
18	OBR	71			47.6		.0066 to .0077	OD							302.4	299.3			Yes	No		
19	IBR	72			47.6		.0015 to .0021	OD								298.6			Yes	No		
20	R(1)	72	105	137.9	47.6	.0016 to .0017		OD	1.655	.0238	.889	0689	0731	290.3		298.7			Yes	No		
21	R(2)	72	105	344.7	47.6	.0007		CC	4.139	.0594	2.222	0903	1338	305.4		307.6			Yes	No		
22	R(3)	72	.105	689.5	47.6	.0005		CC	8.281	.1189	4.444	1641	2344	350.7	378.2	322.6			Yes	No		
23	IAR	72			47.6		.0018 to .0023	OD						357.3	375.1	336.5			Yes	No		
24	OAR	73			47.6		.0014 to .0023	OD						364.6	346.5	336.5			Yes	No		
25	R(1)	164	.227	689.5	47.6	.0043		CC	8.281	.1189	4.444	1351	3192	344.3	782.7	350.6	.0801	.0786	No	Yes	107	
26	R(1)	74	.227	137.9	47.6	.0018 to .0022		OD	1.655	.0238	.889	0627	0951	313.7		314.3			Yes	No		
27	R(2)	74	.227	344.7	47.6	.0005		CC	4.139	.0594	2.222	0772	2144	326.2	434.8	333.7			Yes	No	34	
28	R(3)	74	.227	689.5	47.6	.0004		CC	8.281	.1189	4.444	1441	4026	376.8	371.8	364.3			Yes	No	25	
29	IAR	74			47.6		.0012 to .0020	OD						379.3	425.9	397.1			Yes	No		
30	R(1)	161	.349	689.5	47.6	.0071		CC	8.281	.1189	4.444	0951	5550	318.2	519.8	335.9	.0815	.0800	No	Yes	110	

(b) δ_f = 0.611 rad, f_{no} = 360 Hz

Item	Condition	Correlate number	α_{nom}, rad	$P_{t_1 nom}$, N/cm²	f_n, Hz	ζ_f	ζ_{fs}	Damping measurement	p_{t_2}, N/cm²	p_∞, N/cm²	q_∞, N/cm²	p_u, N/cm²	p_ℓ, N/cm²	T_u, °K	T_ℓ, °K	T_g, °K	$\Delta\delta_{frms}$, rad	$\Delta p_{\ell rms}$, N/cm²	Trip used	Rubber used	Correlation computer data time, sec	Comments
1	IBR	131			350		.0068	CC						326.8	346.2	343.7			No	No	30	
2	R(1)	131	0	344.7	350	.0187		CC	4.139	.0594	2.222			329.3	351.2	344.8	.0049	.0048	No	No	35	
3	R(2)	131	0	689.5	350	.0092[m]		CC	8.281	.1189				353.4	367.6	350.9	.0070	.0069	No	No	35	
4	IBR	136			350		.0052	CC						323.2	342.9	341.2			No	No	35	
5	R(1)	136	.105	344.7	350	.0155		CC	4.139	.0594	2.222			327.6	353.4	344.3	.0049	.0048	No	No	35	
6	R(2)	136	.105	689.5	350	n		CC	8.281	.1189	4.444			340.4	370.4	338.3	.0042	.0041	No	No	35	
7	IBR	112			350		.0012	CC						321.2	302.1	318.2			No	Yes	50	
8	R(1)	112	.105	344.7	350	.0077		CC	4.139	.0594	2.222	.1041	.1186	325.9	305.4	318.7	.0056	.0055	No	Yes	38	
9	R(2)	112	.105	689.5	350	.0214[m]		CC	8.281	.1189	4.444	1503	2048	343.4	337.9	328.4	.0091	.0083	No	Yes	35	
10	IBR	123			350		-.0001[o]	CC						317.6	337.3	336.8			No	Yes	50	
11[p]	R(1)	123	.227	344.7	350	.0347		CC	4.139	.0594	2.222			326.8	358.4	343.7	.0042	.0041	No	Yes	30	
12	R(2)	123	.227	689.5	350	0112		CC	8.281	.1189	4.444			326.8	439.0	364.3	.0049	.0048	No	Yes	30	
13	IBR	119			350		.0080	CC						301.8	282.3	310.7			No	Yes	30	
14[p]	R(1)	119	.227	344.7	350	-.0014[o]		CC	4.139	.0594	2.222	0972	5012	367.5	293.7	301.8	.0049	.0048	No	Yes	30	
15	IBR	127			350		.0021	CC						322.6	343.4	339.3			No	Yes	90	
16	R(1)	127	.349	344.7	350	0200		CC	4.139	.0594	2.222			324.6	365.1	347.9	.0049	.0048	No	Yes	35	
17	R(2)	127	.349	689.5	350	0505		CC	8.281	.1189	4.444			337.9	433.2	386.4	.0084	.0083	No	Yes	35	

Comments (rows 13–15): Tunnel valve may not have opened completely

Footnotes at end of table.

TABLE 1.— HYPERSONIC TEST RESULTS AND DERIVED PARAMETERS — Continued
(M_{nom} = 7.3, V_∞ = 1353 m/sec,[a] T_{0ave} = 962° K,[b] Δp_{urms} < 0.007 N/cm²[c])

(c) δ_f = 1.047 rad, f_{no} = 47.3 Hz

Item	Condition[d]	Correlate number[e]	α_{nom}, rad[f]	$p_{t_1 nom}$, N/cm²[b]	f_n, Hz	ζ_f[g]	ζ_{ls}[g]	Damping measurement[h]	P_{t_2}, N/cm²[a]	P_∞, N/cm²[a]	q_∞, N/cm²[a]	P_u, N/cm²[i]	P_ℓ, N/cm²[i]	T_u, °K	T_ℓ, °K	T_g, °K	$\Delta\delta_{frms}$, rad[j]	$\Delta p_{\ell rms}$, rad[j]	Trip used	Rubber used[k]	Correlation computer data time, sec[l]	Comments
1	R(1)	17	0	68.9	45.4	0.0012 to 0001		OD	0.828	0.0119	0.444								Yes	No		
2	IAR	17			45.4		.0011 to 0015	OD											Yes	No		
3	R(1)	154	0	689.5	47.6	.0040		CC	8.281	1189	4.444	0.1910	0.1993	346.5	366.2	349.3	0.0780	0.0765	No	Yes	125	
4	OBR	54			43.5		.0043 to 0065	OD							299.0	295.9			Yes	No		
5	IBR	55			43.5		.0038 to 0064	OD							298.7	295.8			Yes	No		
6	R(1)	55	0	68.9	43.5	0033 to 0060		OD	.828	0119	.444	.0655	0614	287.9	304.3	295.7			Yes	No		
7	R(2)	55	0	137.9	43.5	0022		CC	1.656	0238	.889	0634	0696	310.7	312.3	297.6			Yes	No	45	
8	R(3)	55	0	344.7	43.5	0015		CC	4.139	0594	2.222	1048	1386	322.9	334.0	307.3			Yes	No	50	
9	IAR	55			43.5		0021 to .0027	OD						325.9	330.5	307.9			Yes	No		
10	OAR	56			43.5		.0023 to 0024	OD						338.2	337.9	329.0			Yes	No		
11[q]	R(1)	151	.105	689.5	47.6	0152		CC	8.281	1189	4.444	0448	2758	346.5	366.2	349.3	0815	0800	No	Yes	88	
12[q]	R(1)	158	.105	689.5	47.6	0065		CC	8.281	1189	4.444	.1489	3737	333.7	438.7	334.8	0801	0786	No	Yes	182	
13	OBR	57			43.5		.0031 to .0036	OD						302.4	318.2	318.0			Yes	No		
14	IBR	58			43.5		0029 to 0035	OD						300.4	316.5	313.4			Yes	No		
15	R(1)	58	.105	68.9	43.5	0028 to 0031		OD	.828	0119	.444	0634	0683	302.4	324.6	313.2			Yes	No		
16	R(2)	58	.105	137.9	43.5	.0017		CC	1.656	.0238	.889	.0593	1027	312.3	338.7	312.9			Yes	No	45	
17	R(3)	58	.105	344.7	43.5	.0023		CC	4.139	0594	2.222	.0855	2075	345.9	377.6	327.1			Yes	No	57	
18	IAR	58			43.5		00099 to .0013	OD						349.3	376.2	338.2			Yes	No		
19	OAR	59			43.5		.0020 to 0022	OD						348.2	340.4	333.4			Yes	No		
20	OBR	41			43.5		0010 to 0044	OD							300.1	296.8			Yes	No		
21	IBR	42			43.5		0015 to 0018	OD							299.0	296.8			Yes	No		
22	R(1)	42	.105	344.7	43.5	.0079		CC	4.139	.0594	2.222			292.3	314.6	329.8			Yes	No	62	
23	R(2)	42	105	689.5	43.5	r		CC	8.281	.1189	4.444			314.6	353.7	389.8			Yes	No	94	
24	IAR	42			43.5		0012 to .0053	OD						355.9	370.7	376.8			Yes	No		
25	OAR	43			43.5		0009 to 0010	OD						367.9	360.7	360.1			Yes	No		
26[s]	R(1)	145	.227	689.5	47.6	0300		CC	8.281	1189	4.444	.1262	6543	328.2	455.8	344.3	0871	.0855	No	Yes	118	
27[s]	R(1)	148	.227	689.5	47.6	.0211		CC	8.281	1189	4.444	1303	.6633	333.4	494.8	336.5	0892	.0876	No	Yes	129	
28	IBR	47			43.5		0013 to 0022	OD						292.1	308.4	306.8			Yes	No		
29	R(1)	47	.227	68.9	43.5	.0014		CC	828	0119	.444	0696	.0979	295.7	321.5	320.4			Yes	No	70	Shadowgraph shows residual hinge rubber flapping
30	R(2)	47	227	137.9	43.5	0013		CC	1.656	0238	.889	0662	1538	304.8	352.3	345.1			Yes	No	57	
31	IAR	47			43.5		0005 to 0019	OD						353.4	393.7	388.4			Yes	No		
32	R(1)	142	.349	689.5	47.6	0129		CC	8.281	.1189	4.444	.1007	8963	324.8	492.3	348.3	0892	.0876	No	Yes	128	
33	OBR	50			43.5		0008 to 0010	OD							305.1	302.1			Yes	No		
34	IBR	51			43.5		0007 to 0011	OD							303.4	302.3			Yes	No		
35	R(1)	51	.349	68.9	43.5	0015 to 0026		OD	.828	.0119	.444	.0683	.1434	294.0	320.1	319.6			Yes	No		Strain gage signal went off paper early in run

Footnotes at end of table.

TABLE 1.– HYPERSONIC TEST RESULTS AND DERIVED PARAMETERS – Concluded
$(M_{nom} = 7.3,\ V_\infty = 1353\ \text{m/sec},^{[a]}\ T_{0ave} = 962°\ K,^{[b]}\ \Delta p_{urms} < 0.007\ \text{N/cm}^{2[c]})$

Item	Condition[d]	Correlate number[e]	α_{nom}, rad[f]	$p_{t_1 nom}$, N/cm²[b]	f_n, Hz	ζ_f[g]	ζ_{fs}[g]	Damping measurement[h]	p_{t_2}, N/cm²[a]	p_∞, N/cm²[a]	q_∞, N/cm²[a]	p_u, N/cm²[i]	p_ℓ, N/cm²[i]	T_u, °K	T_ℓ, °K	T_g, °K	$\Delta\delta_{frms}$, rad[i]	$\Delta p_{\ell rms}$, N/cm²[j]	Trip used	Rubber used[k]	Correlation computer data time, sec[l]	Comments
								(d) δ_f = 1.047 rad, f_{no} = 153 Hz														
1	IBR	31			153		0.0112	CC							298.4	296.2			No	No	20	
2	R(1)	31	-0.105	1241.0	153	0.0353		CC	1.4899	0.2139	7.998			3?07	306.8	338.2	0.0127	0.0007	No	No	150	
3[t]	R(1)	28	-0	1241.0	153	0154[u]		CC	1.4899	.2139	7.998			309.6		330.4	.0127	.0048	No	No	38	
4[t]	R(1)	34	-0	1241.0	153	0796		CC	1.4899	.2139	7.998			297.1	317.6	329.0	0120		No	No	19	Long sting
5	IBR	37			153		0549	CC								297.9			No	No	50	Long sting
6[t]	R(1)	37	0	1241.0	153	0318[u]		CC	1.4899	.2139	7.998			298.4		327.1	.0127	.0545	No	No	24	Long sting
7	IBR	38			153		0597	CC							288.7		303.7			No	No	40	Long sting
8	R(1)	38	.105	1241.0	153	\		CC	1.4899	.2139	7.998			298.4		368.4	.0141		No	No	9	Broken strain gage, long sting
								(e) δ_f = 1.047 rad, f_{no} = 360 Hz														
1	IBR	183			390		.0146	CC							348.2	346.5			No	No	60	
2	R(1)	183	0	344.7	390	0088		CC	4.139	.0594	2.222	0.1027	0.1241		355.1	347.1	.0021	.0021	No	No	37	
3	R(2)	183	0	689.5	390	w		CC	8.281	.1189	4.444	.2013	.2337		363.2	342.6	.0035	.0034	No	No	65	
4	IBR	100			350		.0128[x]	CC						279.3		295.7			No	No	50	Broken strain gage just before model out
5	R(1)	100	.105	1241.0	350	0111[x]		CC	14.899	.2139	7.998	.2599	.5998	324.6		381.2	.0098	.0097	No	No	40	
6	IBR	186			360		.0108	CC						328.2	345.9	344.3			No	No	60	
7	R(1)	186	.105	344.7	360	0198		CC	4.139	.0594	2.222	.0924	1986	335.1	353.4	347.1	.0028	.0028	No	No	35	
8	R(2)	186	.105	689.5	360	0313		CC	8.281	1189	4.444	.1551	4268	354.2	417.6	405.4	.0084	.0083	No	No	35	
9	IBR	180			390		.0121	CC						332.1	350.6	355.0			No	Yes	50	
10[v]	R(1)	180	.227	344.7	390	0431		CC	4.139	.0594	2.222	0876	3785	336.8	361.5	356.5	.0028	.0028	No	Yes	37	
11	R(2)	180	.227	689.5	390	0224		CC	8.281	1189	4.444	.1269	9963	354.0	443.1	369.0	.0091	.0090	No	Yes	34	
12[v]	R(1)	187	.227	344.7	390	0508		CC	4.139	.0594	2.222	.0862	.3730	336.5	358.4	349.8	.0028	.0028	No	Yes	35	
13	IBR	177			350		.0134	CC							344.8	338.0			No	Yes	50	
14	R(1)	177	349	344.7	350	0489		CC	4.139	.0594	2.222	.0758	.6950	334.3	376.2	362.1	.0028	.0028	No	Yes	48	
15	R(2)	177	.349	689.5	350	0806		CC	8.281	1189	4.444	.0752	4879	364.5	490.7	347.6			No	Yes	6	

[a]Determined from table 1 in reference 8 for M_{nom} = 7.3, T_{0nom} = 962° K, and $p_{t_1 nom}$ as listed, with caloric corrections in charts 10, 12, 13, and 20 of reference 8.

[b]The nominal parameters specified for the tunnel operation were considered sufficiently accurate in the hypersonic test, except that the average reservoir temperature T_{0ave} was 962° K, with a range from 834° K to 1077° K, rather than the nominal value of 1055° K.

[c]Deduced because the pressure cell gave a signal in the tunnel which was lower than the instrument noise level, which corresponded to 0.007 N/cm² or less, but gave a distinguishable signal in the jacket of the quick insert mechanism with the cooling air on

[d]OBR means out of jacket before run. IBR means in jacket before run. R(1), R(2), R(3) mean first, second, and third pressures ($p_{t_1 nom}$) during run, if that many; IAR means in jacket after run. OAR means out of jacket after run

[e]Number assigned to a tape data segment. With the table arranged according to increasing values of α_{nom}, the chronology is determined entirely by the increasing order of correlate numbers.

[f]For negative angles of attack, the flap faces the tunnel wall that supports the quick-insert strut. For positive angles of attack, the flap faces the other wall.

[g]For flap damping with flow (ζ_f) and also for flap damping with still air (ζ_{fs}), the damping is measured with high pass and low pass filters set at f_n. When a range of ζ_f values given (for two oscillograph decays), that range is shown as two points in figure 9

[h]CC means damping determined by the correlation computer and OD by oscillograph decays

[i]Recorded (with calibrations) by Beckman equipment for Ames 3.5 Foot Hypersonic Wind Tunnel.

[j]Given only for cases in which the trip mechanism was not used.

[k]Silicone rubber was sometimes placed across the gap at the flap hinge line to protect the strain gage from high stagnation temperature

[l]Data having the shortest data time for a given ζ_f and f_{no} is considered the least reliable if all else is equal

[m]The least squares curve fit was poor for all values of ζ_f and ζ_{fs} in table 1(b) except those marked by m.

FOOTNOTES FOR TABLE 1 – Concluded.

ⁿFor an item where the damping value is not given (because of low signal level in table 1(b)), the remaining data for that item is still presented as part of a survey for catastrophic flutter.

ᵒPoor least squares fit is indicated by the fact that a correlation computer cannot give a negative (unstable) damping.

ᵖItems 11 and 14 constitute a repeatability check on ζ_f except for unexplained differences in T_u, T_ℓ, and T_g (silicone rubber used and trip not used for both items).

�q Items 11 and 12 constitute a repeatability check on ζ_f except for unexplained difference in T_ℓ (silicone rubber used and trip not used for both items).

ʳFor an item where the damping value is not given (because of a poor least squares curve fit in table 1(c)), the remaining data for that item is still presented as part of a survey for catastrophic flutter.

ˢItems 26 and 27 constitute a repeatability check on ζ_f (silicone rubber used and trip not used for both items).

ᵗThe difference in ζ_f for items 3 and 4 may be due to the short sting versus the long sting, and that for items 4 and 6 may be due to $\alpha = -0°$ versus $\alpha = +0°$.

ᵘAll values of ζ_f and ζ_{fs} in table 1(d), except those marked by u, were determined with a low signal level and/or neighboring modes that could not be filtered.

ᵛFor an item where the damping value is not given (because of a broken strain gage in table 1(d)), the remaining data for that item is still presented as part of a survey for catastrophic flutter.

ʷFor an item where the damping value is not given (because of low signal level in table 1(e)), the remaining data for that item is still presented as part of a survey for catastrophic flutter.

ˣAll values of ζ_f and ζ_{fs} in table 1(e), except those marked by x, were determined with a poor least squares fit or neighboring modes that could not be filtered.

ʸItems 10 and 12 constitute a repeatability check on ζ_f (silicone rubber used and trip not used for both items).

TABLE 2.– TRANSONIC TEST RESULTS AND DERIVED PARAMETERS

(a) $\delta_f = 0.611$ rad, $f_{no} = 47.3$ Hz

Item	Correlate number[a]	α_{meas}, rad[b]	M_{nom}	M_{meas}[b]	f_n, Hz	ζ_{fs}, ζ_f[c]	p_t, N/cm²[b]	p_∞, N/cm²[b]	q_∞, N/cm²[b]	p_u, N/cm²[b]	p_ℓ, N/cm²[b]	T_u, °K[b]	T_ℓ, °K[b]	T_g, °K[b]	$\Delta\delta_{frms}$, rad[d]	Δp_{urms}, N/cm²[e]	Trip used	Correlation computer data time, sec[f]	Comments[g]
1	42				47.0	0.0010											Yes		
2	45	0.0696	0.85	0.853	46.4	.0069	10.79	6.71	3.41	6.38	6.12	301.6	301.4	305.1	0.1192	0.0930	No	114	
3	46	-.0021	.90	.895	47.1	.0055	10.49	6.24	3.50	6.07	5.66	302.9	301.8	306.2	.0982	.0800	No	114	
4	52	.0319	.90	.911	47.2	.0015	10.53	6.15	3.57	5.96	5.64	302.9	302.5	307.3		.0800	No	114	
5	47	.0679	.90	.902	46.8	.0033	10.49	6.19	3.53	5.93	5.65	302.3	302.0	306.5		.1000	No	114	
6	51	.1022	.90	.901	46.9	.0010	10.54	6.22	3.54	5.90	5.68	302.1	302.7	307.3		.1131	No	114	
7	49	.1375	.90	.893	46.8	.0015	10.50	6.24	3.49	5.90	5.69	302.2	302.4	306.9		.1131	No	114	
8	50	.2071	.90	.901[h]	46.8	.0004	10.49	6.20	3.52	5.80	5.77	302.6	302.7	307.1		.1600	No	114	
9	55	.0305	.95	.952	47.8	.0007[h]	10.36	5.78	3.67	5.55	5.20	304.3	303.1	308.3		.0731	No	114	Bad time history, unfiltered
10	53	.1009	.95	.945	47.6	.0005	10.30	5.79	3.62	5.54	5.29	302.8	302.6	307.9		.1062	No	114	
11	54	.1708	.95	.950	47.2	.0034	10.35	5.78	3.66	5.53	5.40	302.9	303.0	308.1		.1462	No	114	
12[j]	58	.0298	.99	1.004			10.32	5.43	3.83	5.41	4.99	305.4	303.2	308.6			No		Bad time history, unfiltered
13	56	.1000	.99	1.001	47.6	.0015	10.32	5.45	3.82	5.28	5.05	305.1	303.0	308.3		.0600	No	114	
14	57	.1700	.99	.994	47.5		10.32	5.49	3.80	5.15	5.17	305.0	303.2	308.4		.0600	No	114	

(b) $\delta_f = 0.611$ rad, $f_{no} = 115$ Hz

Item	Correlate number[a]	α_{meas}, rad[b]	M_{nom}	M_{meas}[b]	f_n, Hz	ζ_{fs}, ζ_f[c]	p_t, N/cm²[b]	p_∞, N/cm²[b]	q_∞, N/cm²[b]	p_u, N/cm²[b]	p_ℓ, N/cm²[b]	T_u, °K[b]	T_ℓ, °K[b]	T_g, °K[b]	$\Delta\delta_{frms}$, rad[d]	Δp_{urms}, N/cm²[e]	Trip used	Correlation computer data time, sec[f]	Comments[g]
1	41				115	.0018											Yes		
2	40	.0328	.90	.900	115	.0083	10.69	6.32	3.58	6.03	5.58	305.4	305.1	310.4	.014[j]	.0800[j]	No	108	
3	39	.1200	.90	.894	115	.0052	10.69	6.37	3.56	5.96	5.64	305.3	305.4	310.7	.0141	.1200	No	108	
4	37	.0305	.95	.952	115	.0146	10.56	5.89	3.74	5.68	5.27	308.2	305.7	311.2	.0077	.0717	No	108	
5	37	.0305	.95	.952	115	.0137	10.56	5.89	3.74	5.68	5.27	308.2	305.7	311.2			Yes	108	
6	38	.1537	.95	.941	115	.0074	10.49	5.93	3.67	5.64	5.45	306.1	305.5	311.1	.0120	.1558	No	108	
7	38	.1537	.95	.941	115	.0087	10.49	5.93	3.67	5.64	5.45	306.1	305.5	311.1			Yes	108	
8	27	-.0749	.99	1.001	115	.0045	11.69	6.16	4.33	6.40	5.41	310.3	307.3	312.9	.0141	.0717	No	108	
9	26	-.0049	.99	1.007	115	.0107	11.64	6.10	4.33	6.17	5.48	310.1	307.2	312.7			Yes	108	
10	28	-.0042	.99	.998	115	.0099	11.68	6.19	4.31	6.19	5.49	310.2	307.4	313.0	.0112	.0717	No	108	
11	25	.0653	.99	1.009	115	.0136	11.63	6.08	4.33	5.98	5.55	309.6	307.2	312.8			Yes	108	
12	29	.0654	.99	.998	115	.0155	11.68	6.18	4.31	6.03	5.51	309.8	307.2	312.8	.0120	.0662	No	108	
13	24	.1525	.99	.998	115	.0064	11.63	6.16	4.29	5.79	5.61	309.1	307.4	312.7			Yes	108	
14	30	.1527	.99	1.000	115	.0049	11.68	6.17	4.32	5.83	5.62	309.5	307.7	313.2	.0162	.0641	No	108	
15	23	.2403	.99	.999	115	.0059	11.62	6.15	4.30	5.54	5.74	307.9	307.6	312.5			Yes	108	
16	31	.2401	.99	.999	115	.0067	11.69	6.18	4.32	5.60	5.74	309.1	308.2	313.1	.0176	.0841	No	108	

[a]Number assigned to tape data segment. With the table arranged according to increasing values of M_{nom}, chronology is determined by the increasing order of correlate numbers.

[b]Recorded and calculated (with appropriate calibrations) by Beckman and Honeywell combination for Ames 6 by 6 –Foot Supersonic Wind Tunnel.

[c]Item 1 is ζ_{fs}, the still-air damping, as determined by two oscillograph decays with a damping range as indicated (the range being shown as a band in figure 10). All other items are ζ_f, the total damping under flow conditions, as determined by the correlation computer (tripped oscillograph decays being undecipherable during flow in the transonic test). Both ζ_f and ζ_{fs} are measured with high pass and low pass filters set at f_n.

[d]Because of strain gage malfunction, the latest correlate for which $\Delta\delta_{frms}$ can safely be given (as determined by the variation of strain with α_{nom}) is correlate 46 (item 3); but the correlator values for ζ_f can be believed as long as the signal is stationary.

[e]The pressure cell corresponding to Δp_{urms} was dead throughout the transonic test.

[f]Data having the shortest data time for a given ζ_f and f_{no} is considered to be the least reliable if all else is equal.

[g]Since the flow stagnation temperatures were only slightly higher than room temperature in the transonic test, there was no protection of the flap strain gage by silicone rubber across the hinge-line gap.

[h]The ζ_f value is questionable because the unfiltered time history (fig. 8(c)) indicates nonstationary shifting of the oscillation mean line.

[i]The ζ_f value and other model parameters are not given because of the apparently highly nonstationary unfiltered time history (fig. 8(d)). The remaining data for item 12 are still presented as part of a survey for catastrophic flutter.
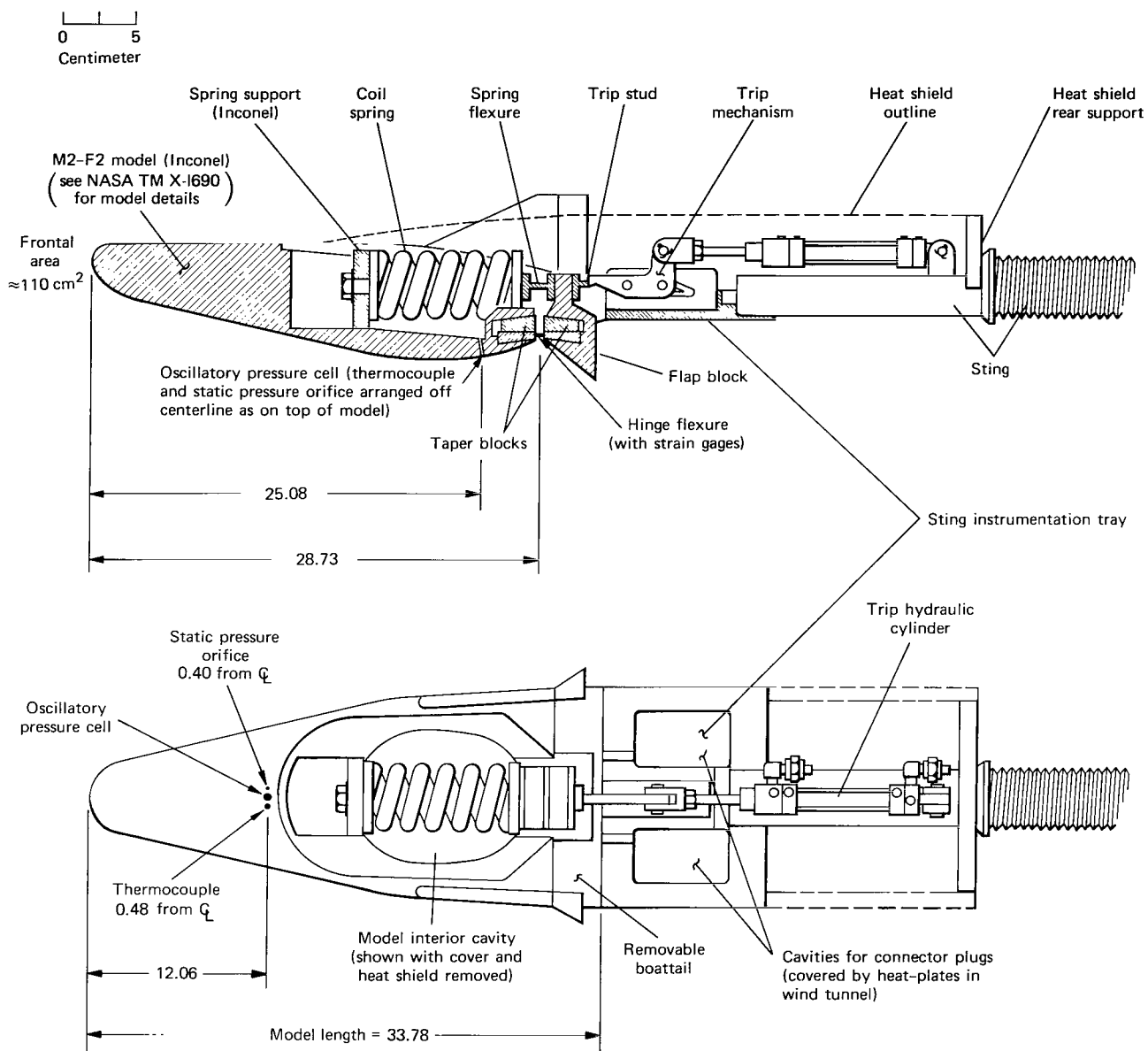
[j]Given only for cases in which the trip mechanism was not used.

23
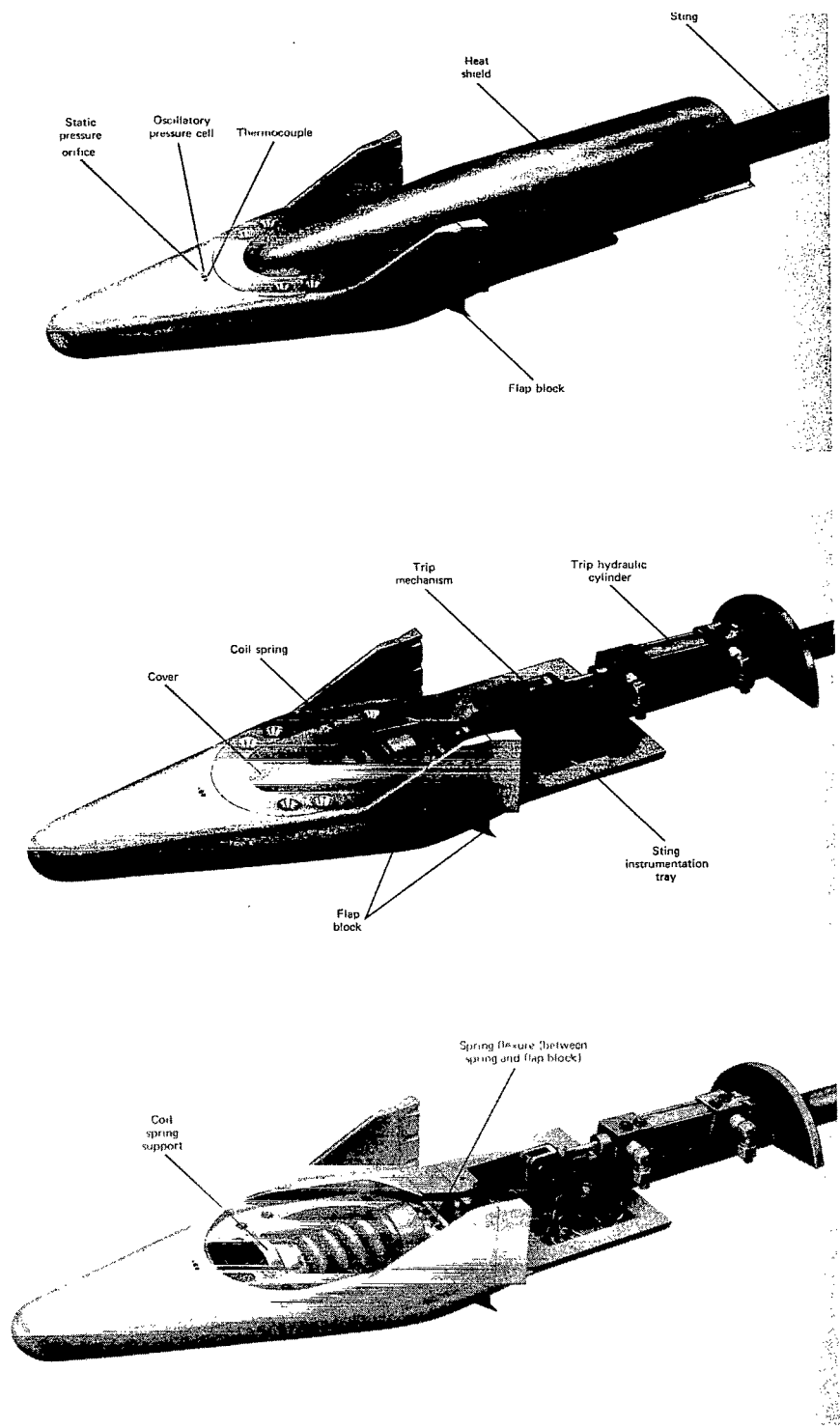
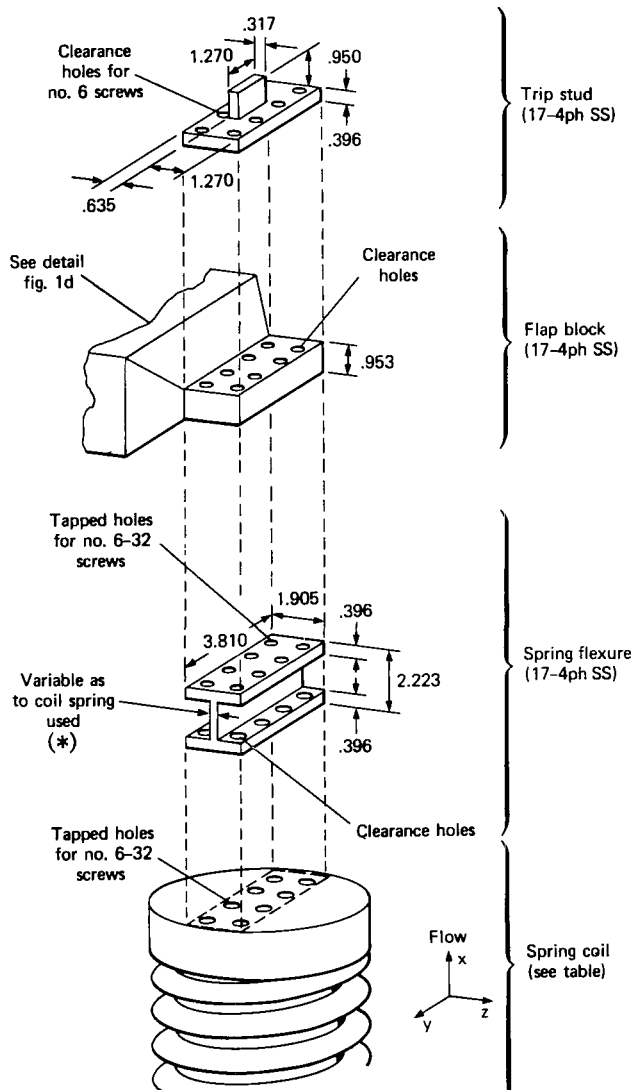(a) Photographs of model assembled and with successive covers removed.

Figure 1.— Model.

(Note: All dimensions are in centimeters)

(b) General drawing.

Figure 1.— Continued.

Wire diameter, cm	0.66	0.94	1.17	1.57
Outside diameter, D, cm	4.44	4.37	4.83	4.80
Number of active coils	7.5	5.2	4.0	3.4
Active coil length, cm	8.25	7.62	6.98	7.39
*Flexure thickness, cm	0.05	0.10	0.10	0.20
k, N/cm	588	4170	—	53,700
f_{n_o}, Hz	47.3	115	153	360

(Note: All dimensions are in centimeters)

(c) Coil spring and spring flexure detail.

Figure 1.— Continued.

		$\delta_f = 0.611$ rad	$\delta_f = 1.047$ rad
f_{n_0}, Hz	k,N/cm	I_{hl} , kg-cm^2	
47.3	588	8.64	9.72
115	4170	10.39	–
153	–	–	–
360	53,700	13.65	14.34

$\Big($ Flap system hinge-line moments of inertia, I_{hl}, kg-cm^2 determined with model assembled $\Big)$
and including effective inertia of coil springs having system stiffness, k,N/cm

$\delta_f = 0.611$ rad $\qquad\qquad\qquad$ $\delta_f = 1.047$ rad

δ_f, rad	(A)	(B)
.611	1.212	4.234
1.047	2.819	3.358
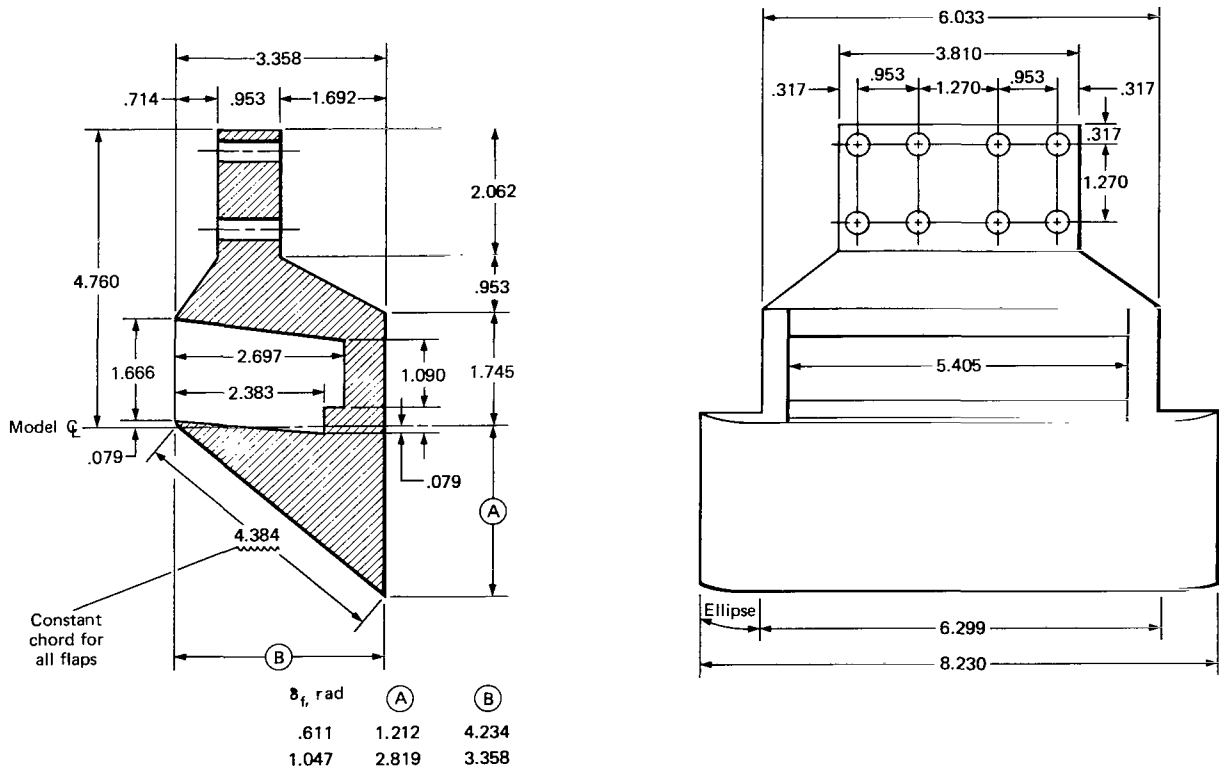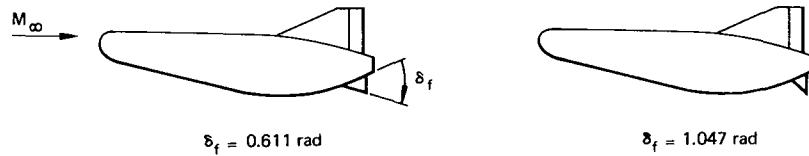
(Note: All dimensions are in centimeters)

(d) Flap block detail.

Figure 1.— Continued.

Passage for
oscillatory
pressure cell

.335 3.429

.317 1.412
.157
.554
.792
2.383
4.879
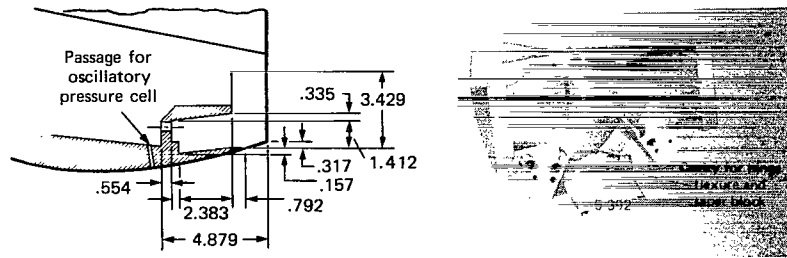
Detail of cavity for hinge
flexure and taper block

Recess for coil
spring clearance

5.397

.953

2.540R

3.096

1.270

2.540
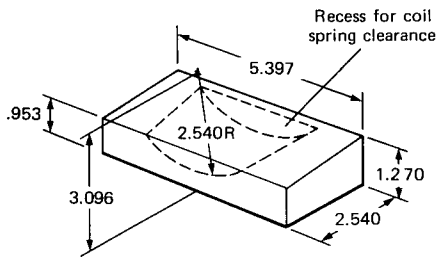
Detail of taper block billets prior to
hand finishing
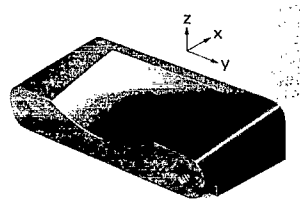
Model-side wedge block
(hand finished to fit cavity)
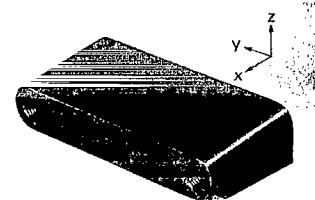
Flap-block-side wedge block
(hand finished to fit cavity)

f_{n_o}, Hz	k, N/cm	t, cm
47.3	588	.025
115	4170	.050
153		.050
360	53,700	.102

Spring flexure: ⊢⊣

Hinge flexure: ⊏⊐

3.607

Flexure spacing

4.775
.239

.635

.239
.396

.792

2.383 2.383

Model
side

Flap block
side

5.397

.554

Model
side

Top view of hinge flexure
showing positions of strain
gages. Gages on center
of flexure length and
located on top and bottom.

Hinge flexure detail
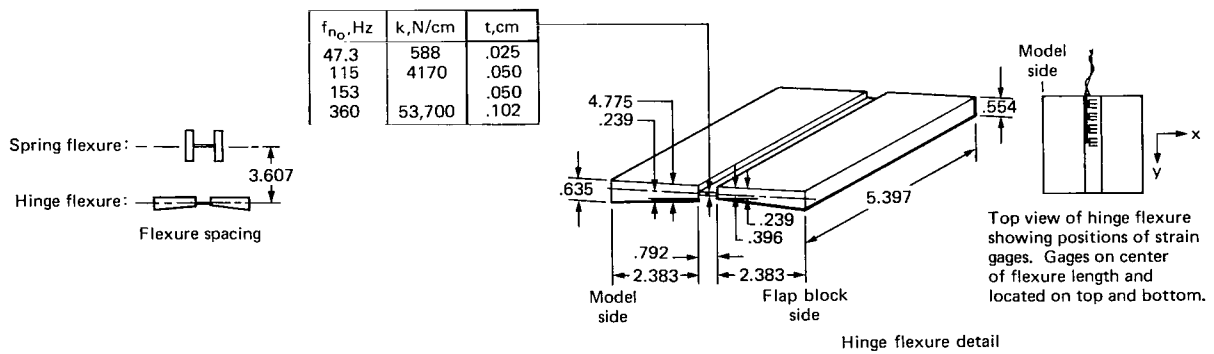
(Note: All dimensions are in centimeters)

(e) Hinge flexure and attachments details.

Figure 1.– Continued.

Center of rotation

Hydraulic cylinder arm connection

.714R

.475 diam

.475R

2.540R

.635

2.540

1.270

.714

.714

.158

1.905

2.540

.953

Press-fit pin location

Slip-fit pin location

Press-fit pin:

Pins .508 diam x 1.587

Slip-fit pin:

Pins .508 diam x .635

Spring recesses
.317 deep x .317 diam,
Spring diam .353

Cam-action slot

Guide slot

.635R

AA   BB

.792

.792

F E

D

.477

2.540R

A

B

C

.477

3.175

1.905

Y

x

1.270

1.905

1.110

1.905

.953

1.905

.794

7.620

(Right hand shown left hand opposite)
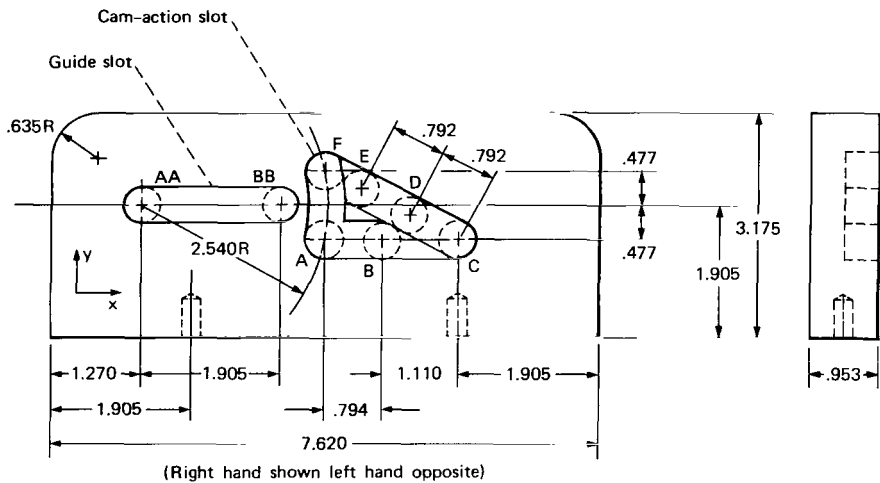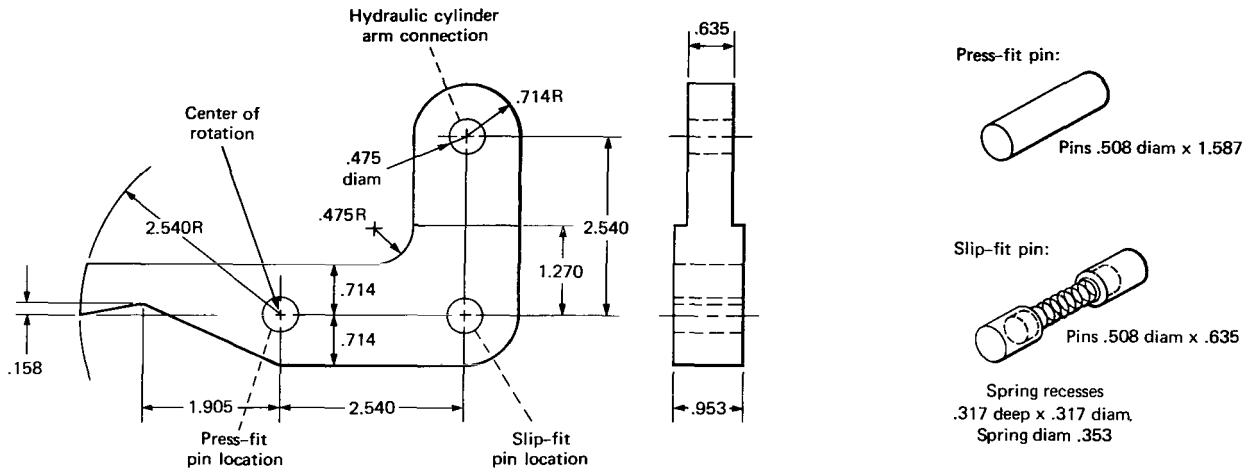
Slots description

Guide slot: From AA to BB .476 deep

Cam-action slot: From point A to point B change from .476 deep
to .317 deep
from point B to point C .317 deep;
from point C to point D change from .317 deep;
to .476 deep.
from point D to point E change from .476 deep;
to .317 deep;
from point E to point F .317 deep;
from point F to point A .476 deep

(f) Trip mechanism details.

Figure 1.— Continued.

Short
sting

Long
sting

25.4 extension

Instrumentation
tray

Tunnel for
lead passage

Hydraulic cylinder
rear support

Sting
3.17 OD x 1.90 ID

Sting jam nut

Heat shield
rear support

2.222

13.810

.236

1.717

3.967

7.302

7.620

11.430

.953

.953

2.222

1.905

.792

3.729

(Note: All dimensions are in centimeters)
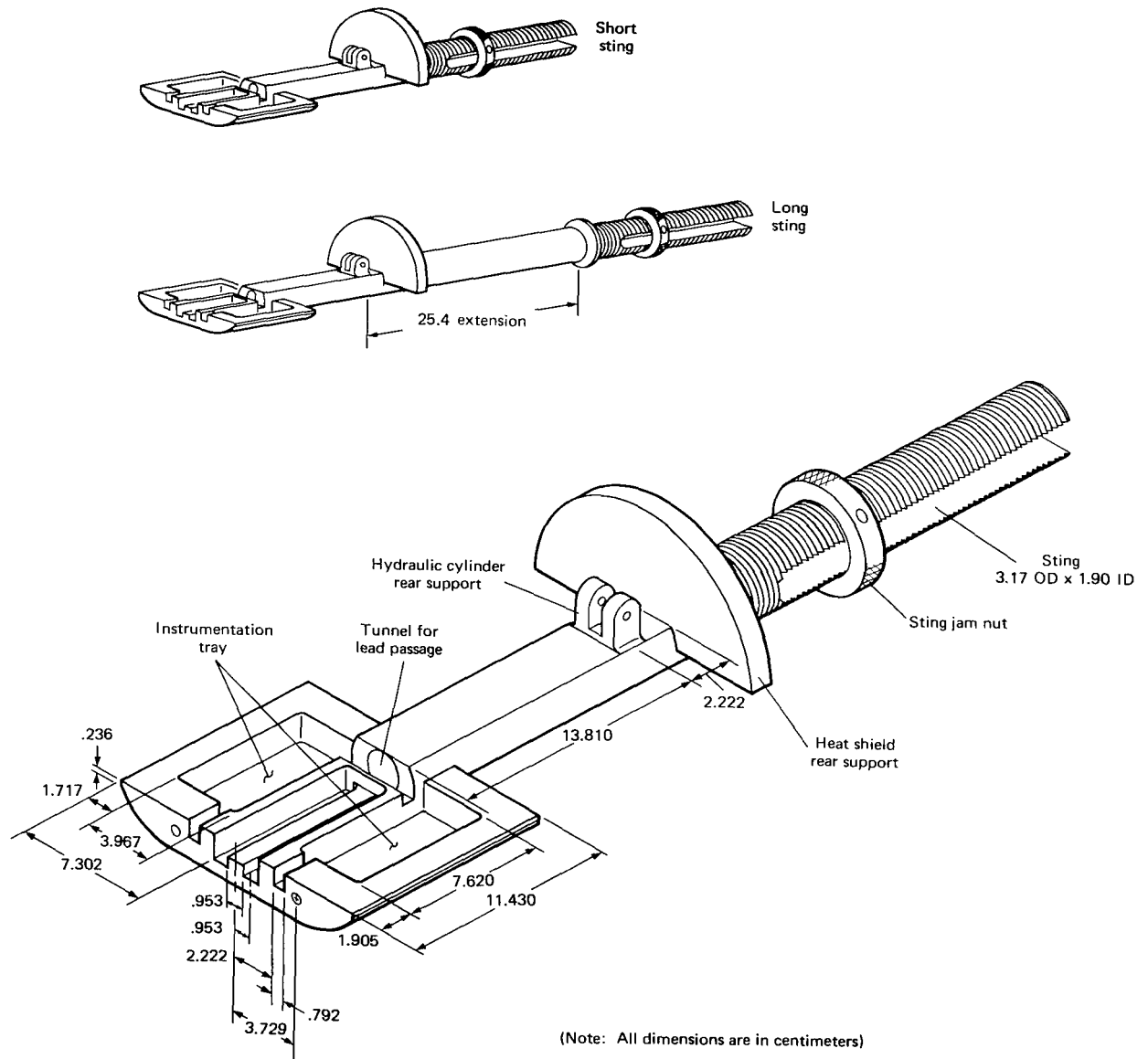
(g) Sting details.

Figure 1.— Concluded.
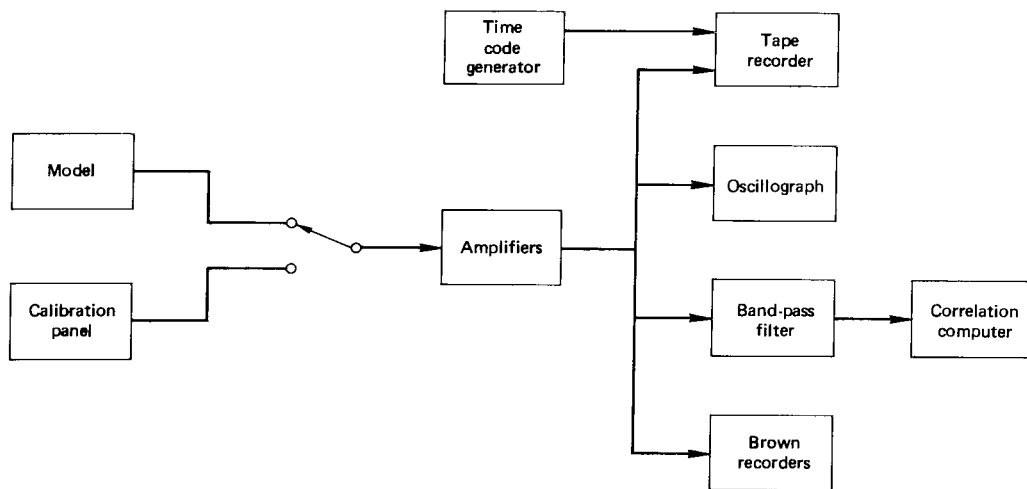
Figure 2.– Block diagram for data recording and monitoring.
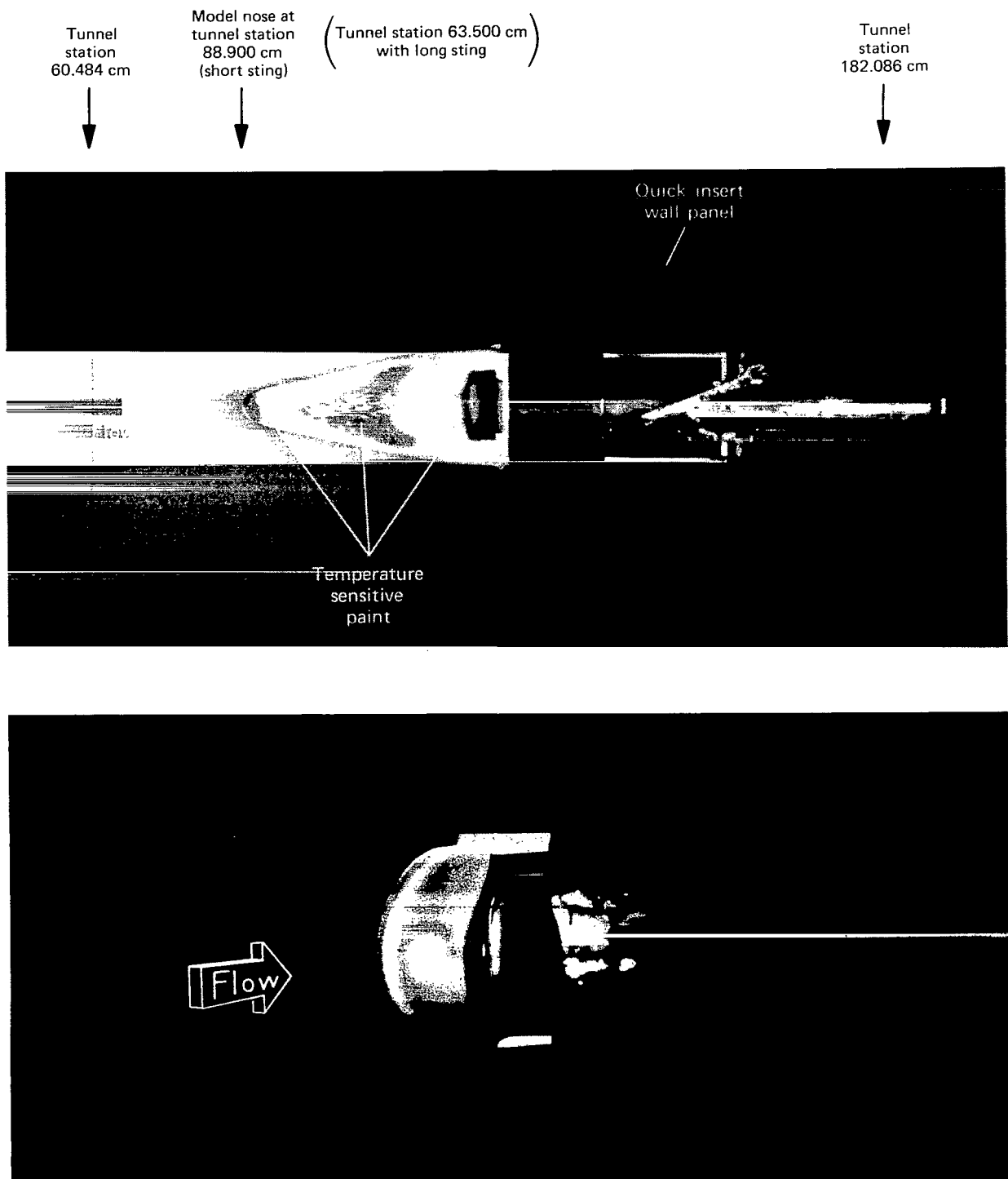
Figure 3.— M2—F2 installation in the Ames 3.5—Foot Hypersonic Wind Tunnel.
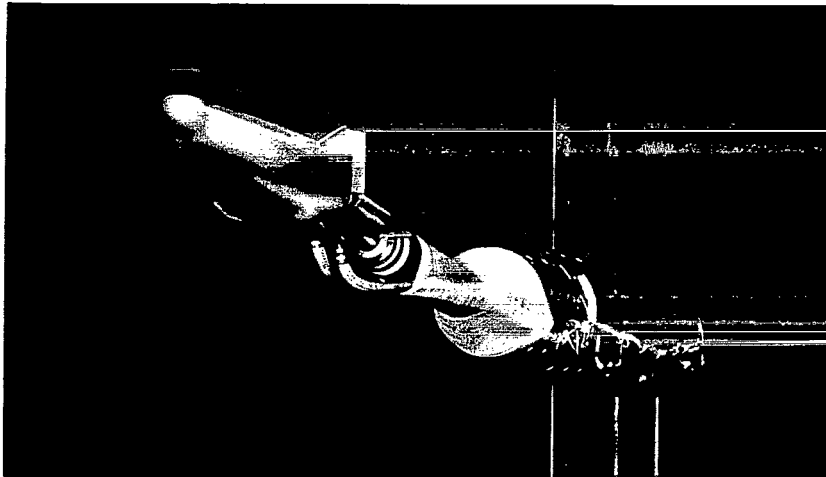
Model nose at tunnel station 2514.9 cm
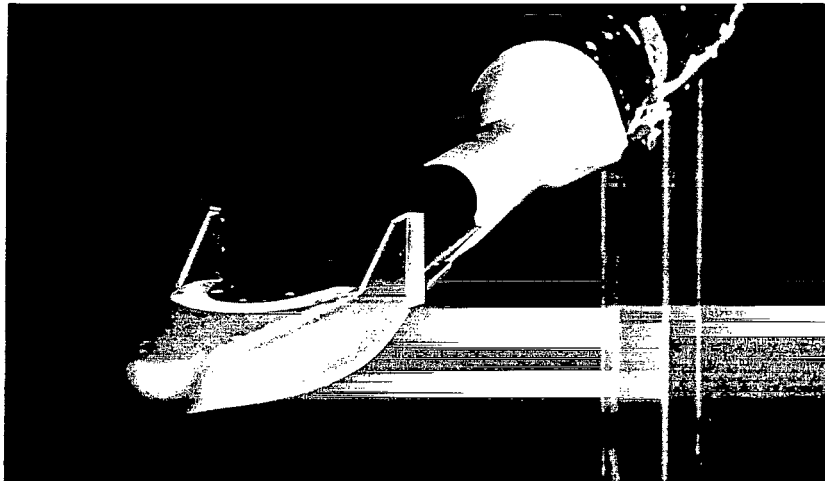
Strut leading edge at tunnel station 2694.9 cm
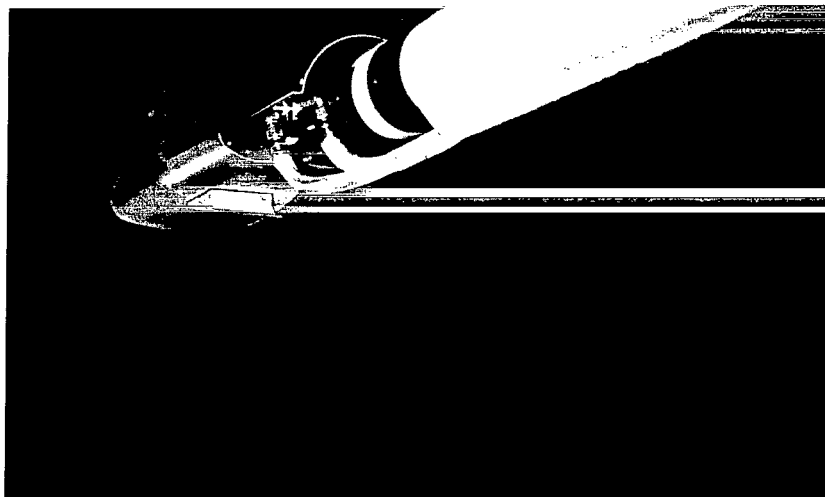
Figure 4.– M2–F2 model installation in the Ames 6- by 6- Foot Supersonic Wind Tunnel.
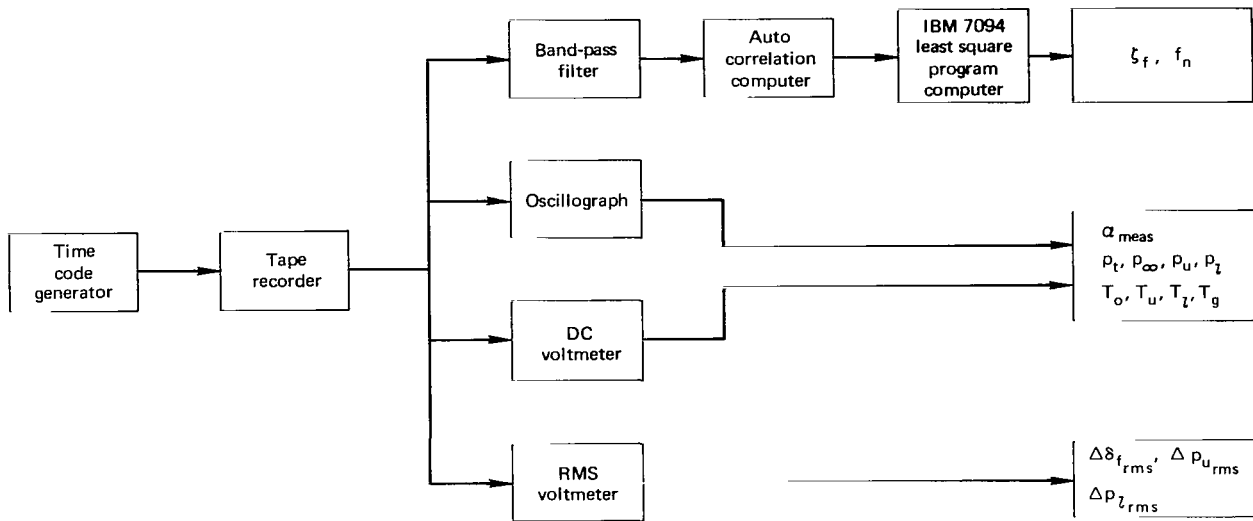
Figure 5.— Block diagram for data reduction.
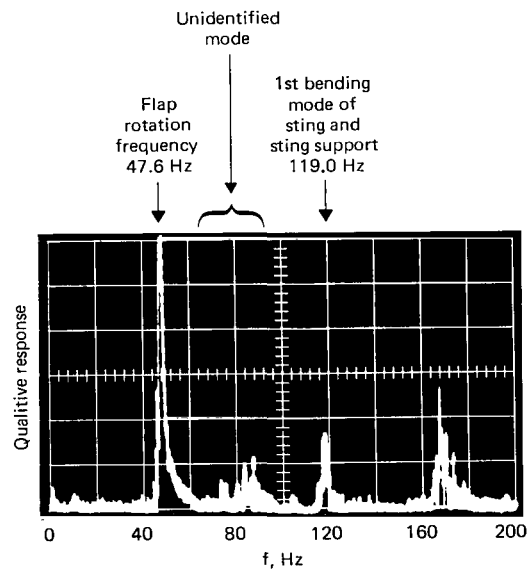
Figure 6.— Unfiltered response spectra for correlate 53, in transonic test.
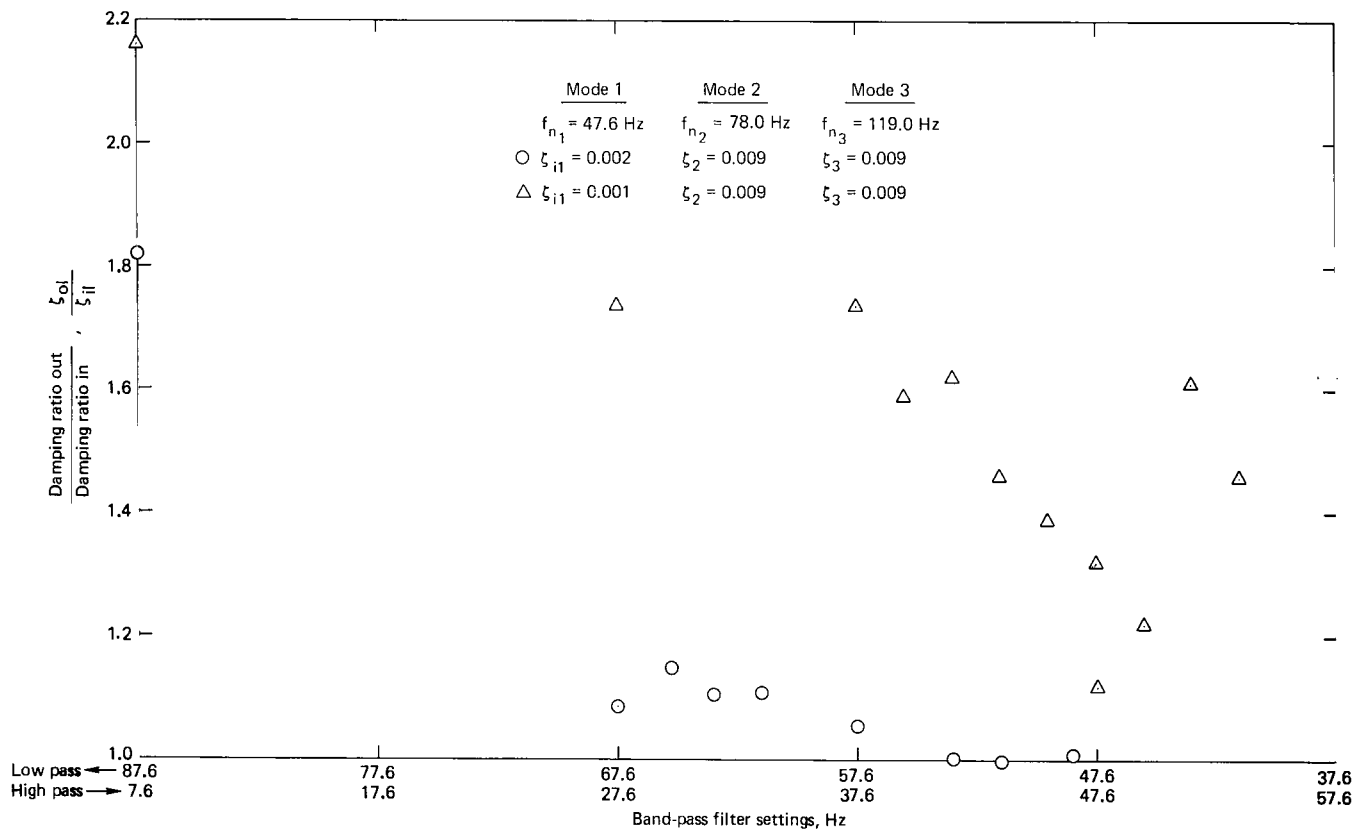
Figure 7.-- Preliminary damping calibration by analog computer simulation.
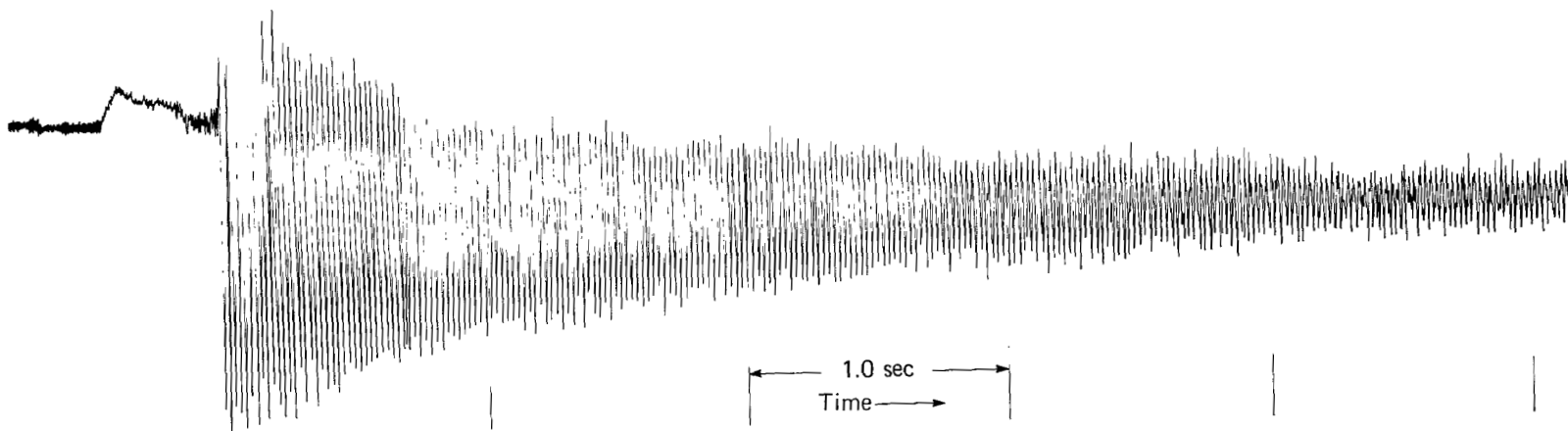
(a) M_{nom} = 7.3, f_{no} = 47.3 Hz, unfiltered (correlate 74, item 28 in table 1(a)) (hypersonic).
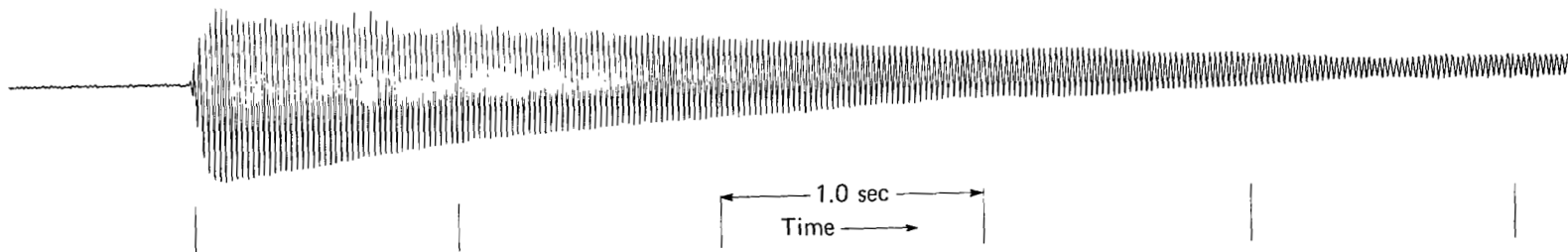
(b) M_{nom} = 7.3, f_{no} = 47.3 Hz, filtered (correlate 74, item 28 in table 1(a)) (hypersonic).

Figure 8.– Data time histories.
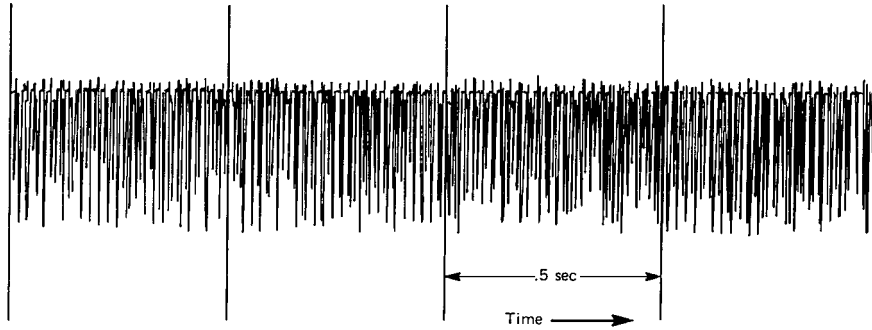
(c) $M_{nom} = 0.95$, $f_{no} = 47.3$ Hz, unfiltered (correlate 55, item 9 in table 2(a), unacceptable for correlator) (transonic).
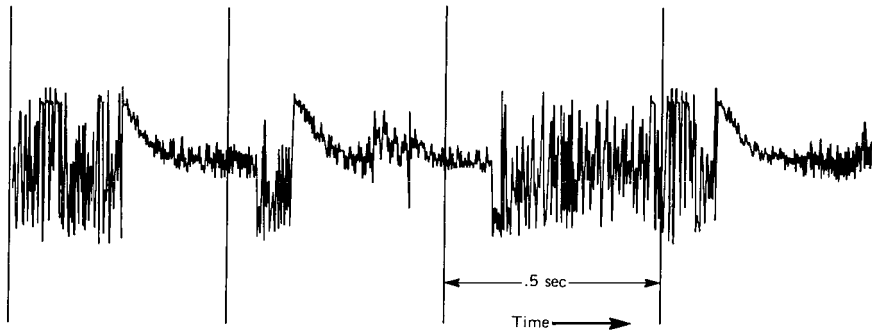
(d) $M_{nom} = 0.99$, $f_{no} = 47.3$ Hz, unfiltered (correlate 58, item 12 in table 2(a), unacceptable for correlator) (transonic).
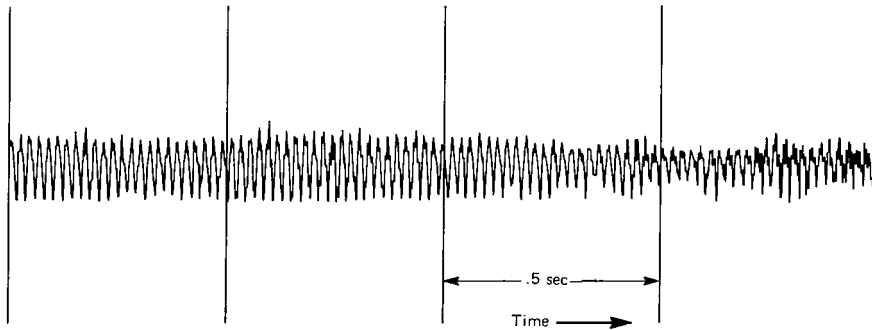
(e) $M_{nom} = 0.90$, $f_{no} = 47.3$ Hz, unfiltered (correlate 50, item 8 in table 2(a), acceptable for correlator) (transonic).

Figure 8.— Concluded.
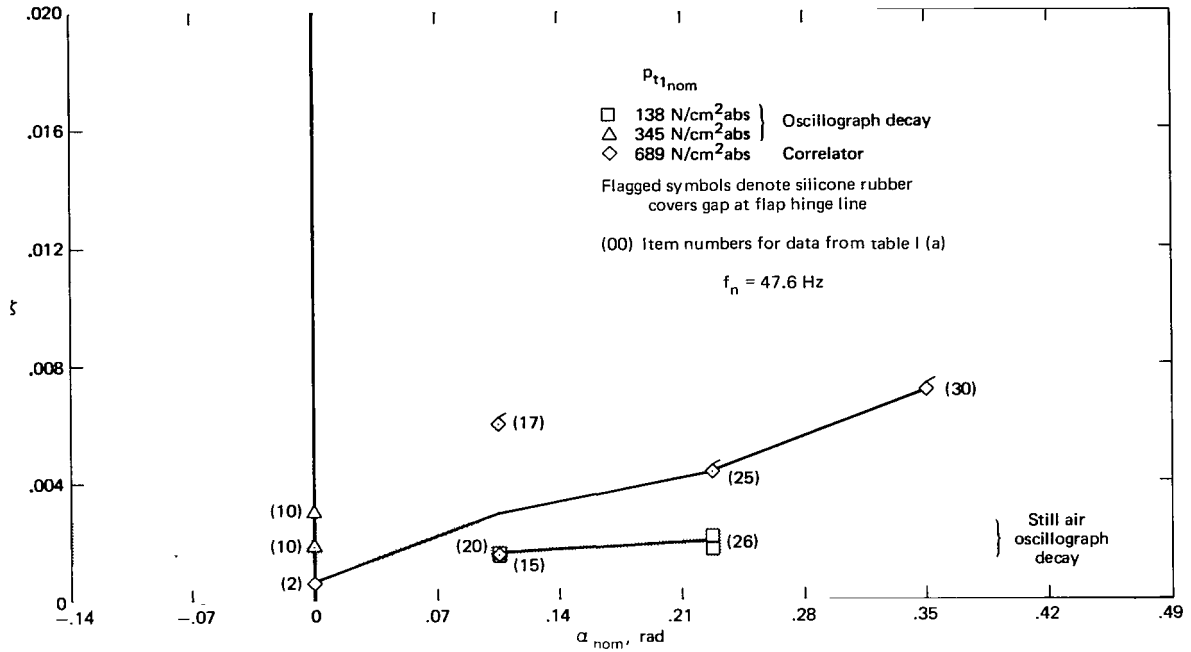
(a) $\delta_f = 0.611$ rad, $f_{no} = 47.3$ Hz
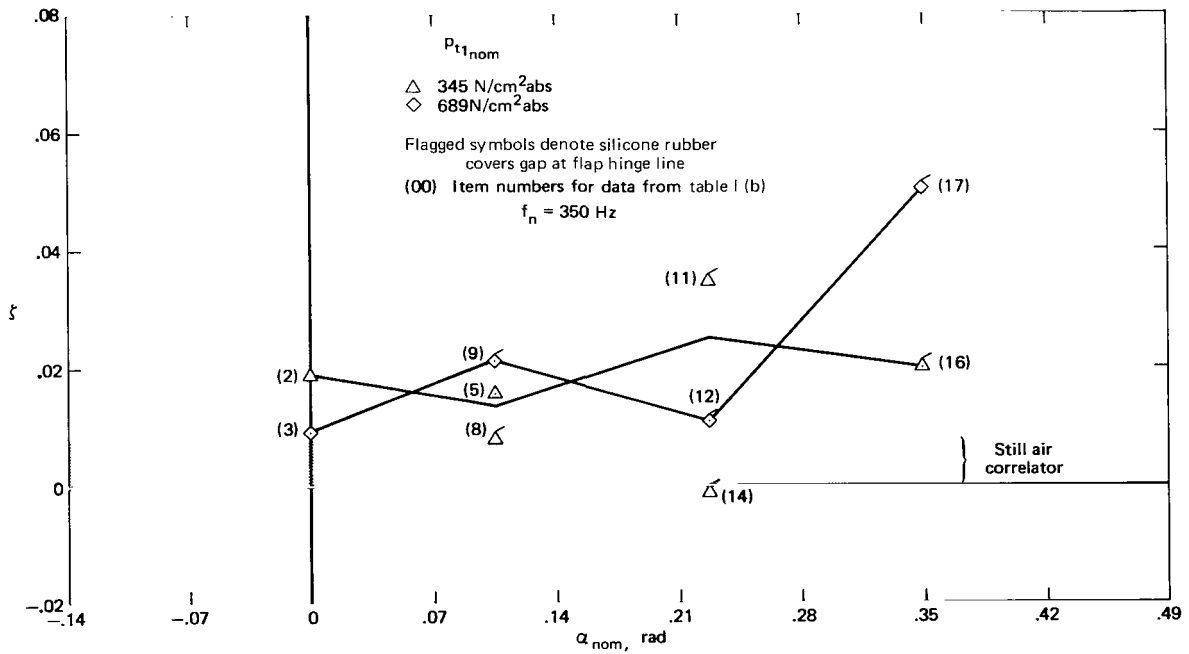
(b) $\delta_f = 0.611$ rad, $f_{no} = 360$ Hz

Figure 9.— Damping results for hypersonic test ($M_{nom} = 7.3$).
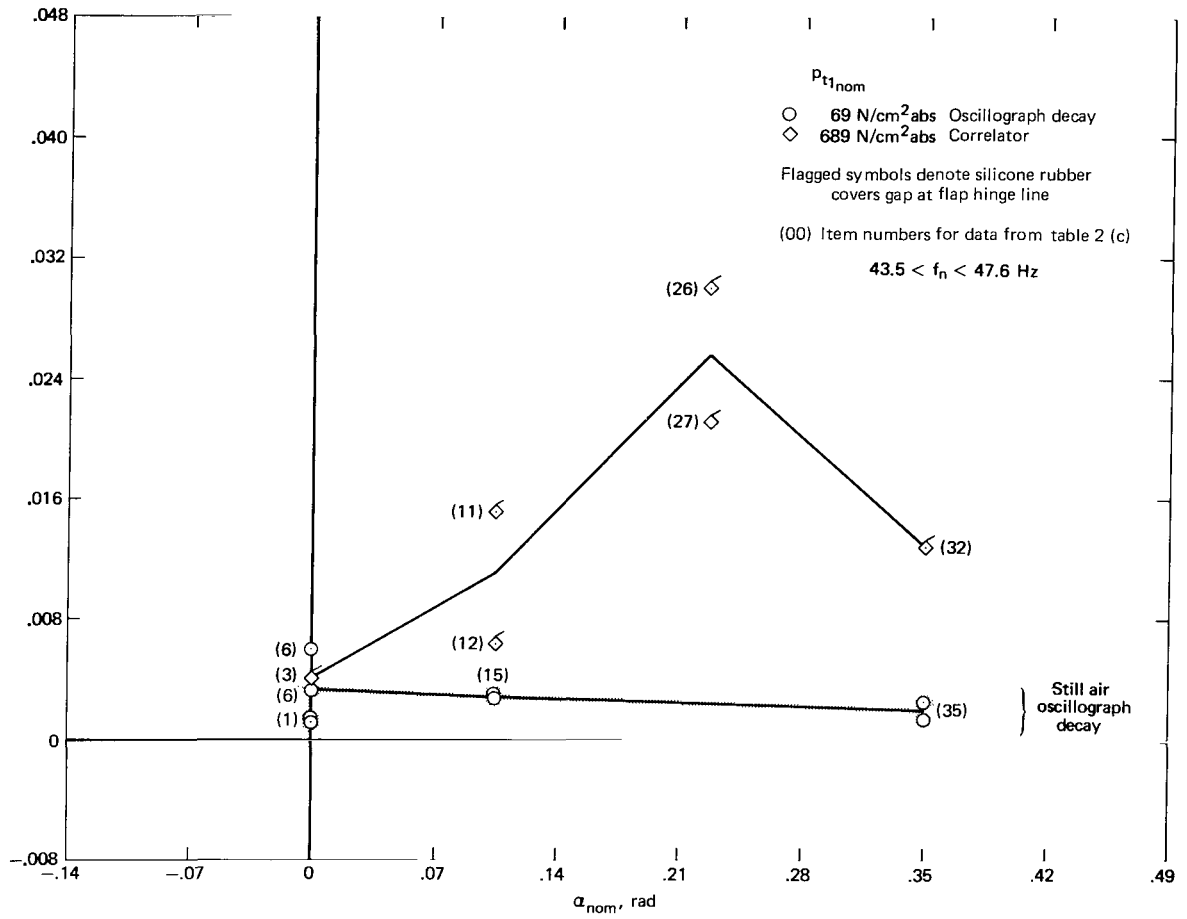
(c) $\delta_f = 1.047$ rad, $f_{no} = 47.3$ Hz

Figure 9. Continued.

40
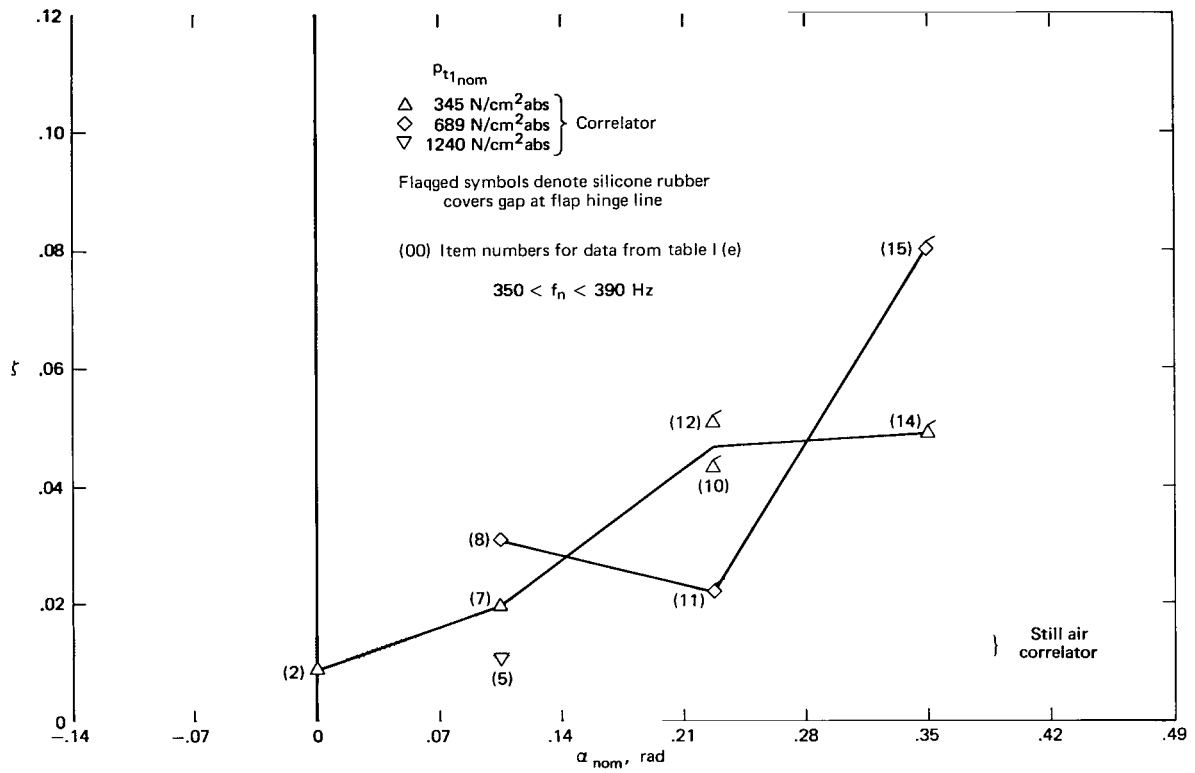
(d) $\delta_f = 1.047$ rad, $f_{no} = 360$ Hz

Figure 9.— Concluded.
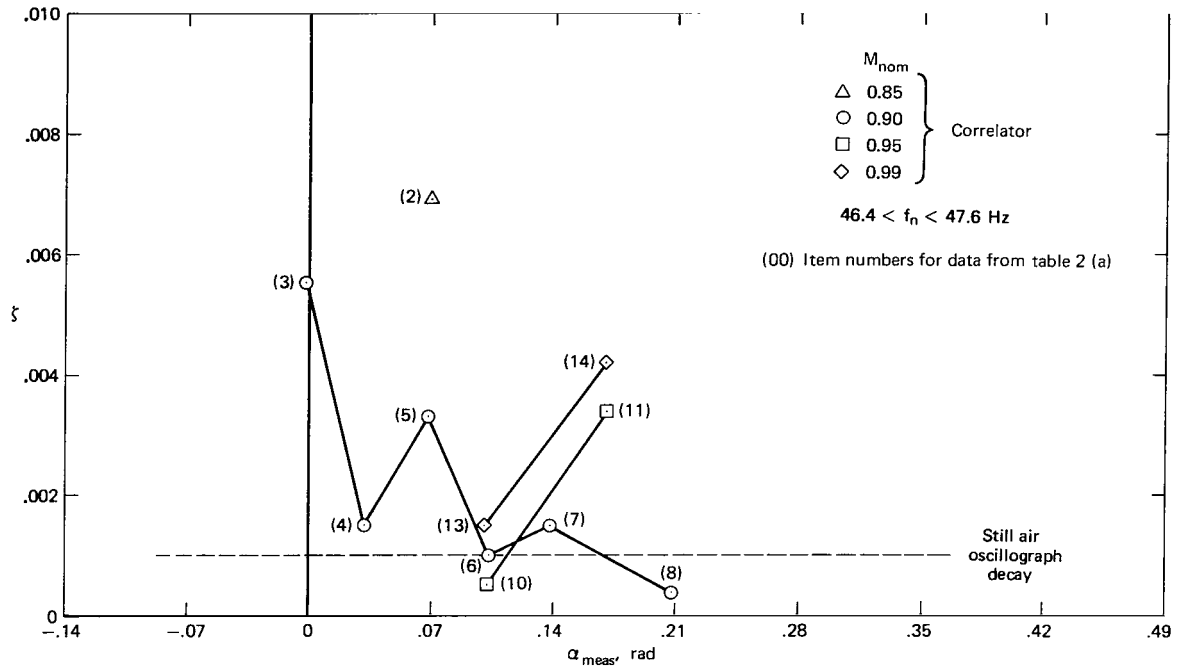
(a) $\delta_f = 0.611$ rad, $f_{no} = 47.3$ Hz
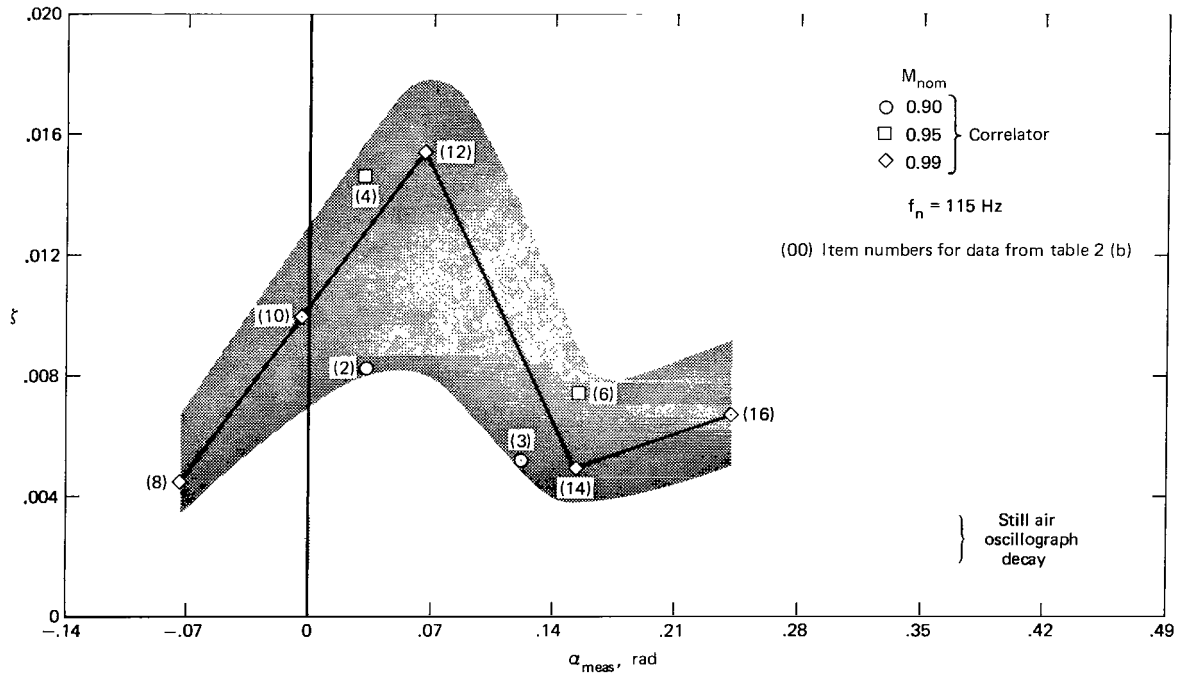
(b) $\delta_f = 0.611$ rad, $f_{no} = 115$ Hz

Figure 10.— Damping results for transonic test.
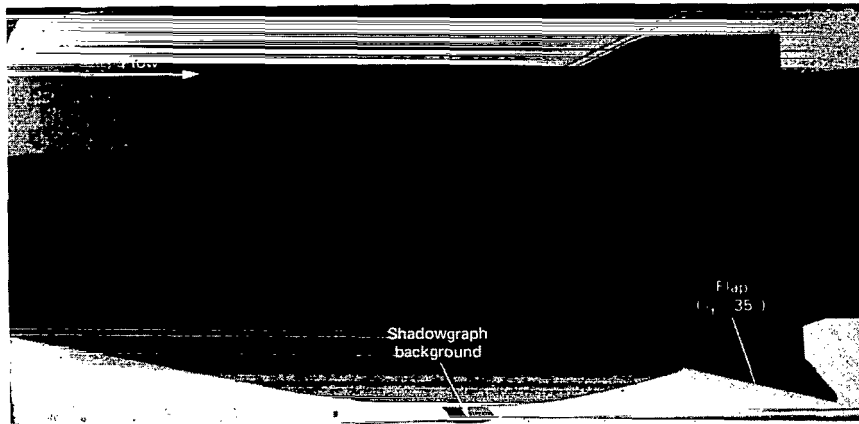
(a) α_{nom} = 0 rad, f_{no} = 360 Hz (item 3 in table 1(b), correlate 131).
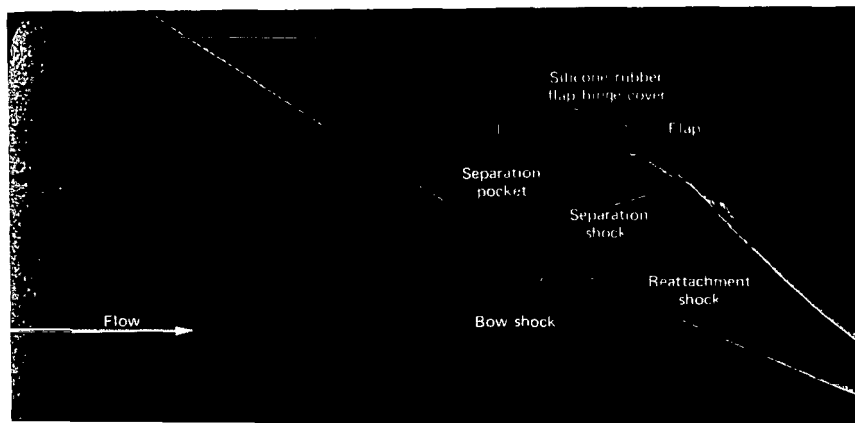
(b) α_{nom} = 0.349 rad, f_{no} = 360 Hz (item 17 in table 1(b), correlate 127).
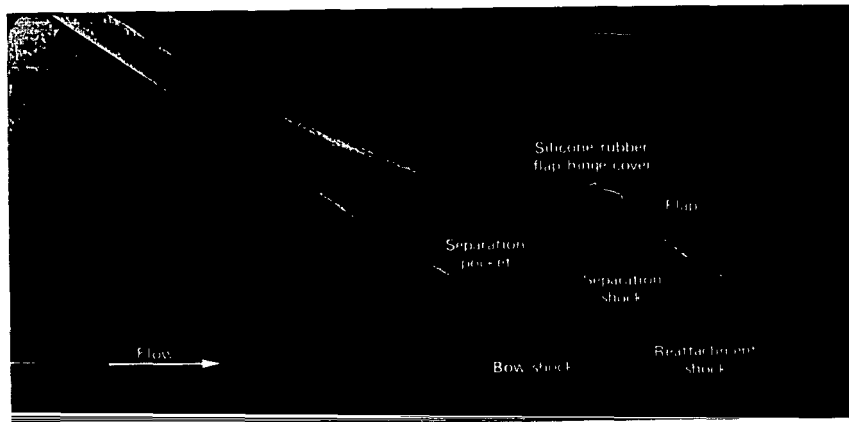
(c) α_{nom} = 0.349 rad, f_{no} = 47.3 Hz (item 30 in table 1(a), correlate 161).

Figure 11.— Shadographs for hypersonic test (M_{nom} = 7.3), δ_f = 0.611 rad, $Pt_{1\,nom}$ = 689.5 N/cm^2 abs.

43
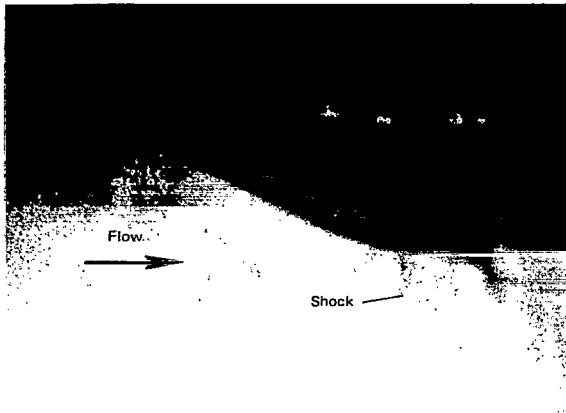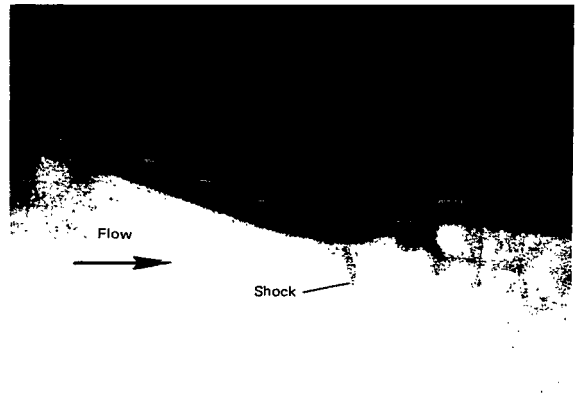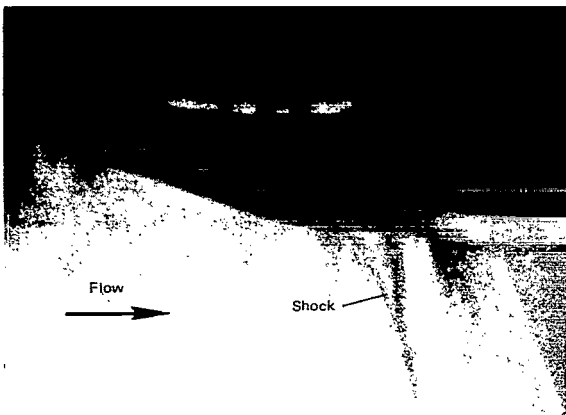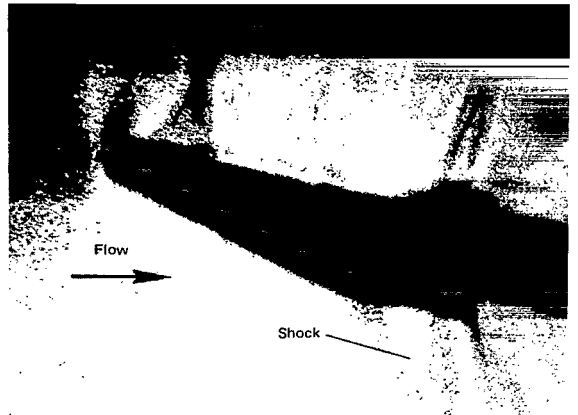
(a) f_{no} = 47.3 Hz, M = 0.9, α_{nom} = 0.210 rad (item 8 in table 2(a)), low damping.
(b) f_{no} = 47.3 Hz, M = 0.9, α_{nom} = 0.068 rad (item 5 in table 2(a)), high damping.
(c) f_{no} = 47.3 Hz, M = 0.95, α_{nom} = 0.105 rad (item 10 in table 2(a)), low damping.
(d) f_{no} = 115 Hz, M = 0.99, α_{nom} = 0.244 rad (item 16 in table 2(b)), high damping.

Figure 12.— Schlieren movie frames for transonic test (δ_f = 0.611 rad).

·"*The aeronautical and space activities of the United States shall be conducted so as to contribute . . . to the expansion of human knowledge of phenomena in the atmosphere and space. The Administration shall provide for the widest practicable and appropriate dissemination of information concerning its activities and the results thereof.*"

— NATIONAL AERONAUTICS AND SPACE ACT OF 1958

NASA SCIENTIFIC AND TECHNICAL PUBLICATIONS

TECHNICAL REPORTS: Scientific and technical information considered important, complete, and a lasting contribution to existing knowledge.

TECHNICAL NOTES: Information less broad in scope but nevertheless of importance as a contribution to existing knowledge.

TECHNICAL MEMORANDUMS: Information receiving limited distribution because of preliminary data, security classification, or other reasons.

CONTRACTOR REPORTS: Scientific and technical information generated under a NASA contract or grant and considered an important contribution to existing knowledge.

TECHNICAL TRANSLATIONS: Information published in a foreign language considered to merit NASA distribution in English.

SPECIAL PUBLICATIONS: Information derived from or of value to NASA activities. Publications include conference proceedings, monographs, data compilations, handbooks, sourcebooks, and special bibliographies.

TECHNOLOGY UTILIZATION PUBLICATIONS: Information on technology used by NASA that may be of particular interest in commercial and other non-aerospace applications. Publications include Tech Briefs, Technology Utilization Reports and Technology Surveys.

Details on the availability of these publications may be obtained from:

SCIENTIFIC AND TECHNICAL INFORMATION OFFICE

NATIONAL AERONAUTICS AND SPACE ADMINISTRATION
Washington, D.C. 20546